Ismael Peruga Nasarre

PHYSICAL WAVEFORM RESEARCH FOR BEYOND 52.6 GHZ IN 5G NR NETWORKS

ABSTRACT

Historically, in order to fulfil all the requirements for the new generations, the frequency bands have been expanded from generation to generation. In particular for the fifth generation new radio (5G NR), where the use of millimetre wave (mmWave) frequencies can offer higher bandwidths, communications in frequencies beyond 52.6 GHz seem really promising and are now under discussion in the 3rd Generation Partnership Project (3GPP) standardisation for the 5G NR future releases. More concretely, both academia and industry are doing research for the frequency range between 52.6 GHz and 114.25 GHz. The reasons why communications beyond 52.6 GHz are interesting is because in those frequencies, high data rate and low latency can be provided due to the large and contiguous channel bandwidth that is available. Also, new use cases can be explored in this frequency range since high accuracy positioning is possible at higher carrier frequencies, such as Orthogonal Frequency Division Multiplexing (OFDM) radar sensing, that allows new kinds of services.

New challenges appear at higher frequencies, or other implementation issues that were not critical in lower frequencies start to become dominant and have to be taken into consideration while defining the new modulations and comparing the possible candidates. The main problems that have to be faced at higher frequencies are the poor propagation conditions (propagation losses are higher than in frequencies below 52.6 GHz), and the radio frequency (RF) impairments that electronic components may have, especially the lower power amplifier (PA) efficiency. Therefore, in order to have a good signal quality, if the peak to average power ratio (PAPR) of the original signal is high, the back-off should be high to make the PA work in the linear region. Thus, the waveform design has to be focused on generating signals with "nearly constant" envelope in order to be able to work closer to the saturation zone of the amplifier without distorting the signal. Also, another problem that has to be taken into account is the large phase noise (PN) present at these frequencies.

The main goal of this work is the comparison between different modulations for discrete Fourier transform (DFT) Spread OFDM (DFTs-OFDM) in order to find a suitable candidate that can be part of the 5G NR communications for carrier frequencies beyond 52.6 GHz, and targeting specially low spectral efficiency (between 1 and 2 bps/Hz). Therefore, the main modulation references are pulse shaped $\pi/2$- binary phase shift keying (BPSK) and quadrature phase shift keying (QPSK) supported in 5G NR Release 15 up link (UL). In this Thesis, several modulation candidates have been tested under realistic conditions by using a 3GPP 5G NR compliant radio link simulator in Matlab. In order to find the best candidate, the waveforms should be able to present good characteristics that can overcome the problems present in mmWave communications.

The main contribution of this Thesis is to propose a new "constrained" phase shift keying (PSK) modulation, called CPSK, which applies a constraint to the symbols that are transmitted in order to reduce the PAPR of the signal. The results have shown that under the mmWave communications conditions (such as low PA efficiency and high PN), the new CPSK modulations can provide significant improvement with the evaluated PA model when compared to QPSK modulation, and together with extensive link level performance evaluations, a clear link budget gain can also be shown for specific CPSK modulation candidates and pulse shaped $\pi/2$-BPSK.

Keywords: DFTs-OFDM, OFDM, waveform, modulation, 5G, NR

The originality of this thesis has been checked using the Turnitin OriginalityCheck service.

PREFACE

Tampereella, 10th December 2019

Ismael Peruga Nasarre

CONTENTS

LIST OF FIGURES

LIST OF TABLES

ix

LIST OF SYMBOLS AND ABBREVIATIONS

3GPP	3rd Generation Partnership Project
ACLR	Adjacent Channel Lekeage Ratio
ADC	Analog to Digital Converter
AWGN	Additive White Gaussian Noise
BER	Bit Error Rate
BLER	Block Error Rate
BPSK	Binary Phase Shift Keying
BS	Base Station
CCDF	Complementary Cumulative Distribution Function
CP	Cyclic Prefix
CP-OFDM	Cyclic Prefix Orthogonal Frequency Division Multiplexing
CPSK	Constrained Phase Shift Keying
CQPSK	Constrained Quadrature Phase Shift Keying
D2D	Device to Device
DFT	Discrete Fourier Transform
DFTs-OFDM	DFT Spread Orthogonal Frequency Division Multiplexing
DL	Down Link
eMBB	Enhanced Mobile Broadband (eMBB)
EVM	Error Vector Magnitude
FFT	Fast Fourier Transform
FR	Frequency Range
IAB	Integrated Access Backhaul
IBO	Input Back Off
ICI	Inter Carrier Interference
iPAPR	Instantaneous Peak to Average Power Ratio
ISI	Inter Symbol Interference
LBG	Link Budget Gain
LDPC	Low-Density Parity-Check
LOS	Line Of Sight

LTE	Long Term Evolution
MCS	Modulation and Coding Schemes
MIMO	Multiple-Input Multiple-Output
mmWave	Millimetre Wave
NR	New Radio
OOB	Out-Of-Band
PA	Power Amplifier
PAE	Power Added Efficiency
PAM	Pulse Amplitude Modulation
PAPR	Peak to Average Power Ratio
PN	Phase Noise
QPSK	Quadrature Phase Shift Keying
RF	Radio Frequency
RMS	Root Mean Square
RRC	Root Raised Cosine
SC-FDMA	Single Carrier Frequency Division Multiple Access
SCS	Sub Carrier Spacing
SE	Spectral Efficiency
SER	Symbol Error Rate
SNR	Signal to Noise Ratio
TR	Technical Reports
UE	User Equipment
UL	Up Link
ZF	Zero Forcing

1 INTRODUCTION

1.1 Context of the project

Currently working wireless networks (fourth generation 4G), have been enough in the last years to fulfil the needs of both customers and industry. However, after the technology evolution occurred in recent years, new services are demanding higher data rates, or lower latency (such as virtual reality, eHealth, autonomous vehicles, ...), hence some new requirements for wireless networks have raised and that is why the 3rd Generation Partnership Project (3GPP), which is the organization that sets the specifications and requirements for mobile networks, decided some years ago to start the development of a new radio access technology, known as fifth generation new radio (5G NR) [1].

Historically, in order to fulfil all the requirements for the new generations, the frequency bands have been expanding from generation to generation, and specifically in 5G, millimetre wave (mmWave) communications in frequencies beyond 52.6 GHz seem really promising and are now under discussion in the 3GPP standardisation of 5G. More concretely, companies and the academy are doing research for the frequency range between 52.6 GHz and 114.25 GHz [2]. For example, in technical reports (TR) [3], [4] or [5], there are some studies about the 60 GHz unlicensed spectrum, channel models for those frequencies, or the next generation access technologies. In TR 38.807 [6], different use cases for frequencies between 52.6 GHz and 100 GHz are shown, as well as the operational and system design requirements.

Communications beyond 52.6 GHz are interesting because in those frequencies, high data rate and low latency can be provided due to the large and contiguous channel bandwidth is available (more than 10 GHz for V-band, around 10 GHz in the E-band and more than 5 GHz around 100 GHz [2]).

Some potential use cases can be mentioned as described in [7]. For example, to alleviate data congestion in lower frequencies for enhanced mobile broadband (eMBB) or provide high data rate eMBB (such as ultra high definition display or augmented reality). Also, applications for smart homes or in offices, such as projections in screens, and different device-to-device (D2D) wireless transmissions. Integrated access back-haul (IAB) is also an important use case for communications in bands above 52.6 GHz, especially in cases when it is not possible or profitable to deploy a wired connection to the 5G base station. Also, new use cases can be explored in this frequency range since high accuracy posi-
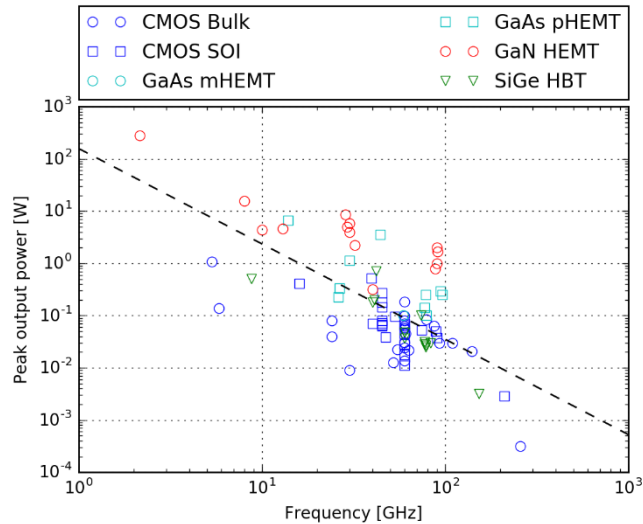
Figure 1.1. *PA output power against frequency*

tioning is possible at higher carrier frequencies, such as Orthogonal Frequency Division Multiplexing (OFDM) radar sensing, that allows new kinds of services.

1.2 Issues and challenges in mmWave communications

New problems appear at higher frequencies or those that were not critical at lower frequencies become problematic. Thus, they must be taken into consideration when defining the new waveforms and modulations to use in this frequency range. Also, when comparing different candidates, the evaluations have to include these implementation issues.

The main issues at higher carrier frequencies are related to the higher propagation loss and frequency dependant atmospheric losses. According to [8], communications beyond 52.6 GHz face from 20 to 40 dB more free space path loss, from 15 to 30 dB/km more atmospheric absorption compared to communications below 6 GHz. Another issues that appear at higher frequencies are the radio frequency (RF) impairments that electronics components may have, specially lower power amplifier (PA) efficiency and higher phase noise (PN) than in lower frequencies. Therefore, in order to have a good signal quality, if the PAPR of the original signal is high, the back-off should be high to make the PA work in the linear region. Thus, the waveform design should be focused on generating signals with "nearly constant" envelope in order to be able to work closer to the saturation point of the amplifier without distorting the signal too much.

In TR 38.803 [9], there is a study of the performance of several PA based on different semiconductor technologies. This study shows that the output power of a PA degrades 20 dB per decade. Thereby indicating that increase in the power capability and in the frequency is not possible simultaneously. This behaviour is shown in Figure 1.1, extracted from the source cited above.

Also, from the same study, the power added efficiency (PAE) is measured for different
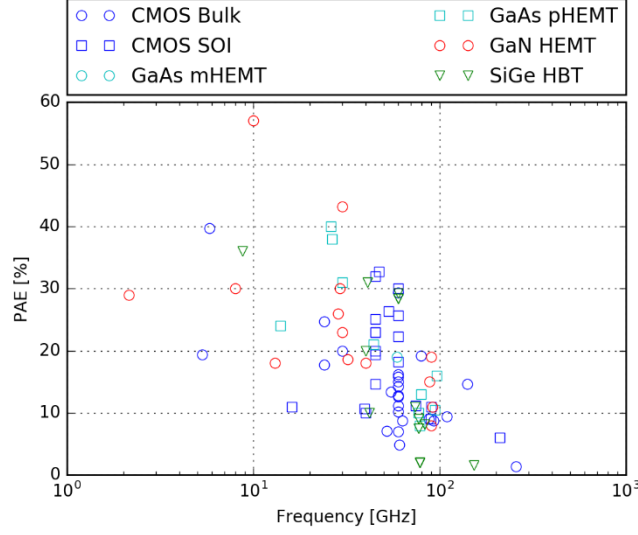
Figure 1.2. *PAE against frequency*

semiconductors technologies, and it can be seen that the efficiency decreases when the frequency increases (see Figure 1.2). The PAE is defined as [9]

$$PAE = \frac{P_{out,RF} - P_{in,RF}}{P_{DC,total}} \tag{1.1}$$

where $P_{out,RF}$ is the output power at radio frequency, $P_{in,RF}$ is the input power at radio frequency and $P_{DC,total}$ is the total DC power.

Seeing the real response of the PA at mmWave frequencies, a non-linear behaviour is expected. Therefore this observation makes necessary the use of a significant power back-off in order to reach the linearity needed to match the requirements, such as adjacent channel leakage ratio (ACLR), fulfil the emission mask, or the error vector magnitude (EVM) requirements [10] for the base station (BS) or [11] for the user equipment (UE).

Apart from the PA non-linearities and low efficiency, the phase noise (PN) can be relatively high at mmWave frequencies. In [12], there is a study on the impacts of PN in the 60 GHz band. The PN is mainly caused by the oscillator, and it can degrade the performance of the communications system, especially with high modulation and coding schemes (MCSs). In [13], the effects of PN on multicarrier communications systems are studied. The PN effects can be divided into two parts: a common phase error (CPE), which is a phase rotation that all subcarriers (SC) inside the same symbol time experience, and inter-carrier interference (ICI), which is a loss of orthogonality between the subcarriers that leads to interference between neighboring subcarriers. According to [9], the PN has the following properties:

- PN increase 6 dB when the frequency doubles.

- PN is inversely proportional to the square of the loaded quality factor of the resonator, Q.

- 1/f noise up-conversion makes the close-to-carrier PN increase (small offset).

To cope with the PN effect, larger subcarrier spacing (for cyclic prefix orthogonal frequency division multiplexing (CP-OFDM) or DFT spread OFDM (DFTs-OFDM)), dedicated reference signals and receiver algorithms can be used to alleviate this problems, or robust modulations can be used.

RF impairments aspect to consider in mmWave communication system design, which are beyond the scope of this thesis, is the noise figure of the RF chain. In high frequencies, in order to have the same noise figure as in low frequencies, the dynamic range of the analog to digital converter (ADC) has to be higher [14] (something that causes high power consumption) and increasing the effective gain of the amplifier causes degradation of the linearity. Also, the RF front end insertion losses have to be taken into account when designing the RF filters.

There are some implementation challenges, as pointed out in [15]. For example the use of digital beamforming, that would require an ADC/DCA for each path, will increase the silicon area and power consumption.

In [7], some system design requirements are explained. Apart from the waveform considerations, already explained in previous lines, beam management has to be studied since large antenna arrays are expected in these frequencies (to cope with the high path loss) and therefore, the beams will be narrow and it requires to improve the beam management.

1.3 Research objectives

The main goal of this project is the comparison between different modulations and waveforms in order to be able to find a suitable candidate that can be part of the 5G NR communications for carrier frequencies beyond 52.6 GHz. In this thesis, several waveform candidates have been tested under realistic conditions by using Matlab. In order to find the best candidate, the waveforms should be able to present good characteristics that can overcome the problems mentioned before.

Of the possible waveform candidates, there are two major groups: single carrier (SC) waveforms and multi-carrier waveforms. One of the most widely used multicarrier waveform is CP-OFDM, currently supported in downlink (DL) and uplink (UL) in NR, as well as in previous generations of communications systems (like Long Term Evolution (LTE) DL [10] or some variants of IEEE 802.11 [16]). In the single carrier waveforms, we can find SC-QAM (which is a pure single carrier waveform) or DFTs-OFDM, also known as single carrier frequency division multiple access (SC-FDMA) in LTE, which is supported in the UL of LTE. Both multicarrier and single carrier waveforms have been compared in this work.

In order to compare the different candidates, they have to be tested under realistic conditions, taking into account the peak to average power ratio (PAPR), the EVM obtained with

a test receiver, and the ACLR after passing through a PA. Also, link level performance evaluations are performed in order to test the robustness of the modulations against PN.

1.4 Methodology

In the development of the thesis, the workflow started with a bibliographic research about basic understanding of 5G in general, and more specifically, the issues that have to be faced in communications with carrier frequencies higher than 52.6 GHz. Also, different proposed solutions in system that faced the same problems (like 802.11ad, 802.11ay or DVB-V2) were revised. A study of different possible waveform candidates and existing solutions for low PAPR modulations were studied, and especially, different techniques and approaches to reduce PAPR for DFTs-OFDM waveforms were implemented and compared. In the bibliographic research, there was a focus on understanding the trade-offs between power efficiency, spectral efficiency and processing complexity.

After having an understanding of the problem statement, the next step was to start developing the Matlab simulator to compare the different waveform candidates. The simulator has been planned to be flexible in order to easily compare different scenarios. At the end of the work, the selected modulations were tested using a 5G NR compliant simulator in order to obtain coded performance. Finally, the numerical results were compared and analysed.

1.5 Structure of the thesis

The thesis is organized as follows. In Chapter 2, the theoretical background needed to follow the thesis is explained, as well as the different solutions already in use in different communications systems with similar problems. In Chapter 3, the different performance metrics used to compare the candidates are presented, as well as the PA and PN models used. In Chapter 4, different techniques to reduce the PAPR that have been used in this project are explained. Chapter 5 shows the modulations that are compared in this thesis. Finally, in Chapter 6, the numerical results are presented and analysed, including peak to average power ratio (PAPR) studies, maximum PA output power per modulation, and coded and uncoded link performance evaluations, finalising with link budget gain (LBG) calculations for the modulations candidates. Finally, Chapter 7 discusses the conclusions and the possible future works.

2 BACKGROUND

In this chapter, the theoretical knowledge needed for all the studied waveforms is given. First, basic single carrier (SC) waveforms are explained, after that, orthogonal frequency division multiplexing (OFDM) is presented and the changes needed to generate a DFTs-OFDM waveform are explained. Also, the different supported waveforms and modulations of systems with similar problems are listed.

2.1 Single Carrier (SC) waveforms

Historically, and still nowadays, single carrier waveforms have been used, due to their simplicity in transmission. The advantages of using pure SC waveforms are that they can achieve a high PA efficiency. This means that the PAPR of this waveforms is low with proper modulation schemes, and that the implementation complexity is relatively simple.

In classical single carrier modulations there is just one carrier frequency carrying (usually) high data rate, which means that the bandwidth of the signal is wide and the symbol duration is short. Single carrier modulations present a peak to average power ratio (PAPR) that can be very small, especially for phase modulations since ideally when using a square pulse they have a constant envelope characteristic [17]. There are different types of SC modulations, pulse amplitude modulation (PAM), phase shift keying (PSK) and frequency shift keying (FSK), each of them modifying the amplitude, phase, or frequency respectively of the signal to carry the information.

The general form of a SC wave is

$$s(t) = A(t)cos(2\pi f_c t + \phi(t)) \tag{2.1}$$

where $A(t)$ is the time varying amplitude and $\phi(t)$ is the time varying phase of the signal. Note that there is only one carrier frequency (f_c).

Pulse Amplitude Modulation (PAM)

The waveform of a digital PAM signal is expressed as [18]

$$s_m(t) = A_m p(t), 1 \leq m \leq M, 0 \leq t \leq T \tag{2.2}$$

Where $p(t)$ is the pulse, with the same duration as the symbol time (T) and A_m belongs

to the group of M possible amplitudes (normally, $A_m = 2m - 1 - M$, with $m = 1, 2, ..., M$).

Since we are describing SC waveforms, the lowpass equivalent presented before is carried by one carrier frequency as

$$s_{m,f_c}(t) = Re\left[s_m e^{j2\pi f_c t}\right] = A_m p(t) cos(2\pi f_c t) \tag{2.3}$$

Phase Shift Keying (PSK)

PSK is a digital modulation that carries the information in the phase. Being M the modulation order. The waveform can be expressed as:

$$\begin{aligned} s_{m,f_c}(t) &= Re\left[p(t)e^{j\frac{2\pi(m-1)}{M}}e^{j2\pi f_c t}\right] \\ &= p(t)cos\left(\frac{2\pi}{M}(m-1)\right)cos(2\pi f_c t) - p(t)sin\left(\frac{2\pi}{M}(m-1)\right)sin(2\pi f_c t) \end{aligned} \tag{2.4}$$

With $m = 1, 2, ...M$ and $\theta_m = \frac{2\pi}{M}(m-1)$ are the M posible values of the phase where the information is sent.

Quadrature Amplitude Modulation

This waveform can be seen as the combination of amplitude with phase modulations. The waveform can be expressed as:

$$\begin{aligned} s_{m,f_c}(t) &= Re\left[r_m e^{j\theta_m}e^{j2\pi f_c t}\right] \\ &= r_m cos(2\pi f_c t + \theta_m) \end{aligned} \tag{2.5}$$

With $r_m = \sqrt{A_{m,i}^2 + A_{m,q}^2}$, being $A_{m,i}$ and $A_{m,q}$ the information bearing signals amplitudes of the quadrature carriers, and $\theta_m = tan^{-1}(\frac{A_{m,q}}{A_{m,i}})$

2.2 OFDM

Orthogonal frequency division multiplexing (OFDM) is the supported waveform for 5G NR in uplink (UL) and downlink (DL). It is a multi carrier waveform, and for that reason several carriers are transmitted in parallel, each of them carrying low bit data rate with a long symbol duration. It is and has been widely used in wireless systems because it is very strong against multipath effects. The main advantage of multicarrier waveforms over single carrier waveform is that, apart from being robust against frequency fading, the channel equalization can be easily performed in the frequency domain when the cyclic prefix (CP) is added, converting the complex task of equalization into simple subcarrier wise complex product.

In OFDM, each subcarrier is modulated with a conventional digital modulation (PSK, QAM, PAM, ...) at a low data rate. However, since there are several subcarriers transmitting at a low data rate, the resulting total rate is analogous to the one that could be achieved with a conventional single carrier modulation.

The property of orthogonality in OFDM is possible since the subcarrier spacing (SCS, Δf) is constant for all the sub carriers, and it is defined as the inverse of the OFDM symbol duration

$$\Delta f = \frac{1}{T} \tag{2.6}$$

This way, if the pulse shape of the sub-symbols (PSK, QAM, PAM) is a rectangular pulse of duration T, the first zero in frequency is at the distance $\frac{1}{T}$ Hz. Therefore, the subcarrier frequencies can be expressed as a function of the subcarrier index n and a reference frequency, f_0 as

$$f_k = f_0 + k\Delta f \tag{2.7}$$

Considering an OFDM waveform with N available subcarriers, the expression of the continuous time OFDM signal is written as

$$s(t) = Re\left[\sum_{i=0}^{N-1}\sum_m x_{m,i}p(t - mT)e^{j2\pi i\Delta ft}e^{2\pi f_0 t}\right] \tag{2.8}$$

where $x_{m,i}$ is the ith symbol of the set $\mathbf{X}_m = [x_{m,1}, x_{m,2}, ..., x_{m,N-1}]$ of (N) complex symbols to be sent in the mth OFDM symbol, T is the duration of the OFDM symbol and $p(t)$ defines the time domain pulse shape. This means that N symbols (from PSK, QAM, PAM modulation) are sent in parallel. Now, if we define

$$a(t) = \sum_{i=0}^{N-1}\sum_m x_{m,i}p(t - mT)e^{j2\pi i\Delta ft} \tag{2.9}$$

Considering just one symbol (m = 1) and rectangular pulse shape, the analytic signal is expressed as

$$a(t) = \sum_{i=0}^{N-1} x_{1,i}e^{j2\pi i\Delta ft}, \quad -T_g \leq t \leq T \tag{2.10}$$

where T_g is the guard interval. Sampling the continuous signal at a rate $T_s = \frac{1}{N\Delta f}$, the resulting sequence has the form:

$$\mathbf{a}_m = a(mT_s) = \sum_{i=0}^{N-1} x_{1i}e^{j2\pi i\Delta fT_s} = \sum_{i=0}^{N-1} x_{1,i}e^{j2\pi \frac{i}{N}} \tag{2.11}$$
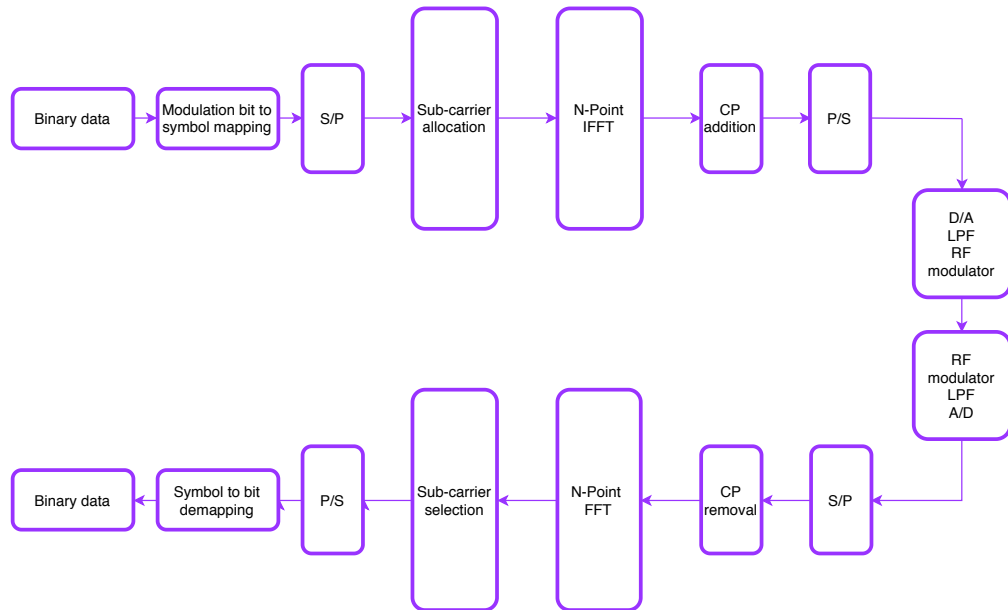
Figure 2.1. *OFDM modulator and demodulator*
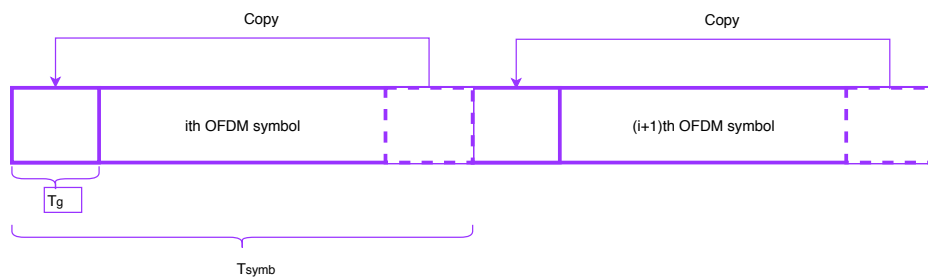
Figure 2.2. *Cyclic prefix in OFDM*

Therefore, it is clear that the sequence a_m (the mth OFDM symbol) can be obtained performing the N-point inverse discrete Fourier Transform (IDFT) of the input complex symbol sequence $\mathbf{X}_m$.

The block diagram of the modulator and demodulator of an OFDM signal is shown in the Figure 2.1.

To overcome the effect of multipath, which causes inter symbol interference (ISI), a cyclic prefix (CP) is added. The CP is a copy of the last part of the OFDM symbol (see Figure 2.2), and it is inserted in the beginning of the symbol in order to have a guard time between 2 successive symbols (the length of the CP should be greater than the maximum delay spread of the channel in order to reduce the ISI) and also to convert the discrete time linear convolution into a discrete time circular convolution. Therefore, the transmission of the signal in the channel can be seen as a point to point product of the DFT frequency samples, making it easy to perform the channel equalization in the frequency domain.

An OFDM symbol is composed by N samples ($\mathbf{a}_i = [a_i[0], a_i[1], ..., a_i[N-1]]$, for the

OFDM symbol i), by adding the CP of μ samples, the OFDM symbol becomes

$$\tilde{\mathbf{a}}_i = [a_i[N-\mu], ..., a_i[N-1], a_i[0], a_i[1], ..., a_i[N-1]]] \tag{2.12}$$

Hence, if $\mathbf{h}_i$ is the channel, the received samples $\tilde{\mathbf{y}}_i$ are

$$\tilde{\mathbf{y}}_i = \tilde{\mathbf{a}}_i * \mathbf{h}_i = \mathbf{a}_i \otimes \mathbf{h}_i \tag{2.13}$$

where $*$ is the convolution operator and $\otimes$ is the circular convolution operator. Which is the circular convolution with the channel $\mathbf{h}_i$. This way, the time convolution between $\tilde{\mathbf{a}}_i$ and $\mathbf{h}_i$ becomes a point to point product in the frequency domain after discarding the CP in time domain. $\tilde{\mathbf{y}}_i$ is obtained as

$$\mathbf{Y}_i = DFT[\mathbf{y}_i] = DFT[\tilde{\mathbf{a}}_i * \mathbf{h}_i] = DFT[\mathbf{a}_i \otimes \mathbf{h}_i] = \mathbf{A}_i \mathbf{H}_i \tag{2.14}$$

Therefore, A_i is easily recovered by means of a well known Zero Forcing (ZF) equalizer after estimating the frequency response of the channel $\mathbf{H}_i$ as the division of the received samples in frequency domain ($\mathbf{Y}_i$) by the estimated channel as

$$\mathbf{A_i} = \frac{\mathbf{Y}_i}{\hat{\mathbf{H}}_i} \tag{2.15}$$

Some advantages and disadvantages of OFDM can be mentioned as pointed in [19].

Advantages

- The main advantage of OFDM is the reduction of inter-symbol interference by the addition of the CP.

- The complexity of the receiver is much lower comparing to a single carrier sytem with time domain equalization.

- The spectral efficiency offered by OFDM is high, due to the fact that it uses orthogonal overlapping subcarriers.

- Since the modulator and the demodulator can be implemented with IDFT and DFT, fast Fourier transform (FFT) algorithms can be used, and therefore, make them more efficient.

- Each subcarrier can be modulated with a different modulation, making the system very flexible.

- Good support for multiple-input multiple-output (MIMO) communications.

- Frequency selective scheduling of multiple users.

- Native support for non-contiguous frequency allocations.
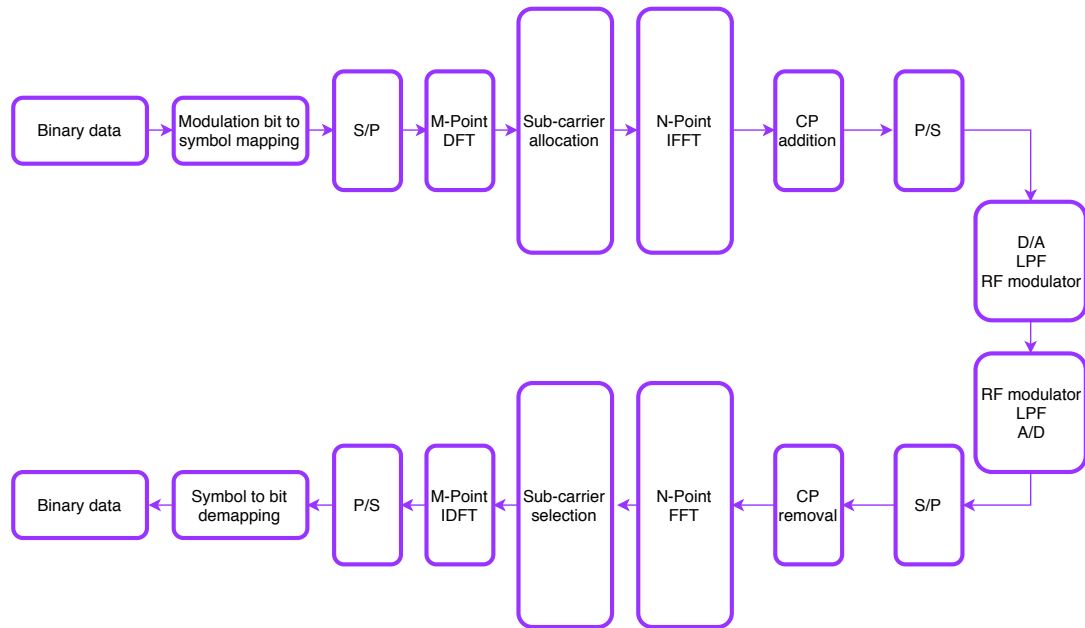
Figure 2.3. *DFTs-OFDM modulator and demodulator*

Disadvantages

- The main disadvantage is the high PAPR presented by OFDM.
- There is a small loss in efficiency when the CP is added.
- Sensitivity to carrier frequency offset.
- Sensitivity to PN.

Since in mmWave communications, one of the most important feature that the waveform should present is a low PAPR, OFDM does not seem a good candidate to be used.

2.3 DFTs-OFDM

DFTs-OFDM (also known as SC-FDMA) is a modification of the OFDM scheme explained before. DFTs-OFDM is used in the UL of 4G LTE in order to make the mobile terminal more power efficient. The main advantage of DFTs-OFDM over OFDM is that DFTs-OFDM presents a lower PAPR, thus making the transmission more efficient.

OFDM and DFTs-OFDM share some processing functions: both use blocks of basic modulation symbols to generate the final OFDM or DFTs-OFDM symbol, also the data is sent on discrete subcarriers, frequency domain equalization can be done and both use the CP to mitigate the ISI caused by multipath propagation.

The basic block diagram of a DFTs-OFDM modulator and demodulator is illustrated in Figure 2.3.

The main difference in the transmitter is the DFT operation added for DFTs-OFDM. This operation spreads the energy of one subcarrier over all allocated subcarriers. The input of the transmitter takes M digital modulated symbols (from PSK, QAM, PAM, ...), then M

symbols are the input for an M-point DFT that generates M frequency domain symbols. After the DFT, the modulator is the same as for basic CP-OFDM. The M symbols are mapped to M subcarriers out of the N available subcarriers distributed in the channel bandwidth (there are different ways to perform the subcarrier mapping, but in this Thesis, only the so-called localized subcarrier mapping is considered. For further reading on subcarrier allocation techniques, see [19]). Following the subcarrier mapping, an N-point IDFT is performed and the samples are converted from parallel to serial to obtain the time domain samples. Before transmission, the CP is added for the same reasons as it is added in OFDM (prevent ISI and convert the linear convolution with the channel into a circular convolution), and optionally, to reduce the out of band emissions, a filtering operation can be done.

To generate the DFTs-OFDM waveform, M complex symbols ($\mathbf{c}$) are taken and an M-point DFT is performed in the first step

$$z_k = \sum_{p=0}^{M-1} c_p e^{-j\frac{2\pi}{M}kp}, \quad k = 0,...,M-1 \tag{2.16}$$

The frequency domain symbols for the DFTs-OFDM symbol m ($\mathbf{Z}_m = [z_1, z_2, ..., z_{M-1}]$) are then modulated as in a regular OFDM modulator, so, the vector $\mathbf{Z}_m$ here is equivalent to $\mathbf{X}_m$ in the OFDM explanation from the previous section (see equation (2.8)). Now, if the expression of z_k is introduced in (2.10) (and changing the sub-index k for i), we get

$$a(t) = \sum_{i=0}^{N-1} \sum_{p=0}^{M-1} c_p e^{-j\frac{2\pi}{M}ip} e^{j2\pi i \Delta f t}, \quad -T_g \leq t \leq T \tag{2.17}$$

Swapping the order of the summation

$$a(t) = \sum_{p=0}^{M-1} c_p \sum_{i=0}^{N-1} e^{j2\pi i \Delta f(t-\frac{p}{M\Delta f})}, \quad -T_g \leq t \leq T \tag{2.18}$$

From the previous expression, the term $\sum_{i=0}^{N-1} e^{j2\pi i \Delta f(t-\frac{p}{M\Delta f})}$ can be seen as the pulse used to shape the c_p symbols. That is why DFTs-OFDM is said to be a single carrier waveform.

The DFTs-OFDM receiver is shown in Figure 2.3. It receives the DFTs-OFDM symbol, removes the CP, performs an N-point FFT operation to recover the N subcarriers, then the M wanted subcarriers are extracted and the frequency domain equalization is done. After that, an M-point IDFT is carried out to transform the samples into time domain and the M modulation symbols are detected.

Although as it has been explained, OFDM and DFTs-OFDM have similarities, the main difference is that in OFDM, a multicarrier signal is transmitted, when in DFTs-OFDM, the signal is SC, therefore DFTs-OFDM presents lower PAPR than OFDM and it is worth it to

take it into account especially in the application studied in this work. For these reasons, DFTs-OFDM is the main waveform to be studied in this thesis.

2.4 Overview of other communications systems with similar requirements

Some of the first waveforms to consider for this project were the ones proposed in communications systems that have to face similar issues, e.g., reduced PA efficiency or increased phase noise. For that reason, systems like IEEE 802.11ad, IEEE 802.11ay or DVB-S2 had been studied and their proposed solutions had been collected to be used as reference points of how they are dealing with the mentioned implementation issues.

2.4.1 Supported modulations and waveforms in IEEE 802.11ad/ay

IEEE 802.11ad is a wireless networking standard that works at 60 GHz carrier frequencies [16], and IEEE 802.11ay is an enhancement of 802.11ad. Thus, these two systems work in the same frequency bands that are of interest for this Thesis.

IEEE 802.11ad supports SC and multicarrier waveforms. All the preambles of the transmitted packets are SC, followed by the payload, that can be either SC or OFDM. For the preamble, the SC modulation used are $\pi/2$-BPSK and $\pi/2$-DBPSK, whereas in the data transmission, in the SC case, the modulations used are $\pi/2$-BPSK, QPSK and 16QAM. In the OFDM case, the modulations used are QPSK, SQPSK, 16QAM and 64QAM. In Table 2.1 all the modulations and waveforms supported in 802.11 are shown for the different Modulation and Coding Schemes (MCS).

Due to the fact that $\pi/2$-DBPSK and SQPSK are not so well known modulations, they are defined here.

$\pi/2$-**DBPSK**
From [16], the encoded bit stream $[c_0, c_1, c_2, c_3...]$ is mapped to non-differential BPSK:

$$\tilde{s}_k = 2c_k - 1 \tag{2.19}$$

Then, the differential sequence $d(k)$ is generated by multiplying:

$$d_k = \tilde{s}_k \times d(k-1) \tag{2.20}$$

Where $d(-1) = 1$, to encode the first bit of the sequence. After the differential mapping,

Table 2.1. *Supported waveforms and modulation schemes in 802.11ad*

MCS	Modulation
Single Carrier (SC)	
0	$\pi/2$-DBPSK
1 - 12	$\pi/2$-BPSK $\pi/2$-QPSK $\pi/2$-16QAM
25 - 31	$\pi/2$-BPSK $\pi/2$-QPSK
OFDM	
13 - 24	SQPSK QPSK 16QAM 64QAM

the sequence is multiplied by a phase rotation factor of $\pi/2$ radians:

$$s_k = d_k e^{j\pi\frac{k}{2}} \tag{2.21}$$

SQPSK

SQPSK stands for Spread QPSK, the basis of this constellation [16], is that the stream of bits is broken into groups of N bits. Each pair of bits of the first $N/2$ bits, is mapped normally to QPSK constellation points, and they modulate half of the OFDM subcarriers.

$$s_k = \frac{1}{\sqrt{2}}\left[(2c_{2k} - 1) + j(2c_{2k+1} - 1)\right] \tag{2.22}$$

The rest of the subcarriers are modulated by the complex conjugate of the previously mapped symbols for the fist half of the subcarriers (s_k^*).

In the enhanced version (IEEE 802.11ay), apart from the previous modulations, it also supports non-uniform constellation ($\pi/2$-64-non uniform constellation) and $\pi/2$-8PSK.

$\pi/$2-64-non uniform constellation

In [20], the $\pi/2$-64-non uniform constellation is defined. This 64-QAM constellation is optimized to maximize the mutual information on AWGN channel, and there it is claimed that this constellation achieves gains between 0.2 and 2.9 dB against uniform 64-QAM under different channels (AWGN, AWGN and PN, or AWGN, PN and PA non-linearities). The constellation and the bit to symbol mapping is illustrated in Figure 2.4

Figure 2.4. *Non-Uniform 64-QAM constellation*

2.4.2 Supported modulations and waveforms in DVB-S2

DVB-S2, Digital Video Broadcasting by Satellite, is the digital TV standard transmission system by satellite [21]. This system does not work in the mmWave frequencies, but faces some similar problems, like the use of highly non-linear PA used in satellite transmitters.

In DVB-S2, there is only support for SC waveforms. The used modulations are QPSK, 8PSK, 16APSK (constellation illustrated in Fig. 2.5) and 32APSK, so, the spectral efficiency varies from 2 to 5 bps/Hz and they provide different possible roll-off factors, which are 0.35, 0.25 and 0.2. The choice of SC waveforms is because they present a quasi constant envelope (QPSK or 8PSK), and when the satellite is transmitting, the power efficiency is high. However, 16APSK and 32APSK are used with quasi-linear transponder (high back off) or by using techniques to compensate the non-linear behaviour.

2.4.3 Supported modulations and waveforms in 5G New Radio Release 15

In the 3GPP 5G NR Release 15, the first specifications of 5G are set. In [10], the BS radio transmission and reception requirements are explained. In the DL, for frequencies below 52.6 GHz, the supported DL waveform is CP-OFDM. There are different types of BS (type 1-C, 1-H, 1-O and 2-O), where the requirements are defined as conducted or radiated, and also the classification depends on the frequency range (FR1, from 410 MHz to 7125 MHz or FR2, from 24250 MHz to 52600 MHz) where the BS is working. The BS type 2-O is the one that is used in FR2, and the supported modulations for this BS type are shown in Table 2.2.

Figure 2.5. *16APSK constellation*

Table 2.2. *Supported waveforms and modulations for 5G Release 15 in the DL*

Waveform	Supported modulation
CP-OFDM	QPSK
	16-QAM
	64-QAM
	256-QAM

In [22] the physical channels and modulations supported by 5G NR are defined. For the UL, both CP-OFDM and DFTs-OFDM are supported. In Table 2.3, the supported modulations and waveforms for the UL are shown.

Table 2.3. *Supported waveforms and modulations for 5G Release 15 in UL*

Waveform	Supported modulation
DFTs-OFDM	$\pi/2$-BPSK
	QPSK
	16-QAM
	64-QAM
CP-OFDM	QPSK
	16-QAM
	64-QAM

3 EVALUATION ASSUMPTIONS AND MODELS

In this chapter, the different performance metrics to compare the waveforms are presented. These metrics evaluate different aspects of the waveform.

3.1 PAPR

Instantaneous (sample wise) PAPR

One of the most important metrics is the instantaneous (sample wise) PAPR (iPAPR) of the waveform because the signal has to be amplified by means of a PA, and large peaks in the signal can cause degradation in the performance if the PA is not used in its linear region. As a consequence, it generates in band distortion which increases the bit error rate (BER) and out of band radiation, that originates adjacent channel interference. As explained in chapter 1, the PA efficiency is low at high frequencies, and the backoff should be large if the PA has to work in the linear region. Thus, signals with low iPAPR are needed for communications beyond 52.6 GHz.

For a complex valued samples of a signal $s[n]$, with $n = 0, 1, ..., N - 1$, the iPAPR can be defined as

$$iPAPR[n] = \frac{|s[n]|^2}{\frac{1}{N} \sum_{k=0}^{N-1} |s[k]|^2} \tag{3.1}$$

After getting the iPAPR for each sample of the signal, the complementary cumulative distribution function (CCDF) is calculated. The CCDF of iPAPR is defined as the probability that the PAPR level X dB is reached, and is defined as

$$Prob(iPAPR > iPAPR_0) \tag{3.2}$$

PAPR per OFDM symbol
The PAPR per OFDM symbol (any type of OFDM symbol, including DFTs-OFDM symbols) is another way of measure the PAPR that has been widely used. In this case, one PAPR value per OFDM symbol is evaluated, and the distribution is obtained by evaluating the OFDM symbol wise PAPR values over a large set of OFDM symbols. This metric does not represent the PAPR of the waveform as accurately as the iPAPR, because it just

takes into account one sample from each OFDM symbol.

Given N samples of OFDM symbol i, the PAPR per OFDM symbol is defined as

$$PAPR_i = \frac{max[|s_i[n]|^2]}{\frac{1}{N}\sum_{k=0}^{N-1}|s_i[k]|^2} \tag{3.3}$$

Once the PAPR per DFTs-OFDM symbol is computed for all the symbols, the CCDF of it is calculated as in the iPAPR case.

3.2 EVM

Error Vector Magnitude (EVM) is a performance metric utilised to measure the performance of a transmitter. It quantifies the difference between the ideal waveform and the received waveform. From the 3GPP specifications for the UE [11], the EVM of DFTs-OFDM can be expressed as

$$EVM = \sqrt{\frac{\sum_{v\in T_m}|z'(v) - i(v)|^2}{|T_m|P_0}} \tag{3.4}$$

where T_m is the set of $|T_m|$ active modulation symbols in the measurement period, $z'(v)$ are the samples of the received signal (symbols of the modulation, this is, after performing the FFT, subcarrier selection and IDFT in the receiver), $i(v)$ are the ideal symbols sent and P_0 is the average power of the ideal signal. Similar method is defined for CP-OFDM.

In order to measure the EVM, first the sent symbols before the DFT in the transmitter are stored to be used as a reference ($i(v)$). After receiving the signal, since the CP was added, there is a range of samples where the quality of the signals would give a value close to the minimum EVM. For that reason, the CP is not directly discarded, but the samples are taken from the middle of the CP. More concretely, the EVM measurement, following the 3GPP specification is performed by taking the receiver FFT starting from two different points within the CP. The EVM is computed for both cases and the maximum between both EVM (low and high) is the final EVM value.

The two different points within a CP are defined through a so-called EVM window. The centre of the window is placed in the centre of the CP and the length of the window depends on the FFT size used. The samples to compute the EVM low (EVM$_l$) are taken from the beginning of the window, and the samples to compute the EVM high (EVM$_h$) are taken from the end of the EVM window. Figure 3.1 illustrates the process to get the samples from the received signal. After getting the samples, the normal receiver is applied (subcarrier selection, equalizer, IDFT). Table 3.1 taken from [11] specifies the EVM window length for normal CP for 120 kHz SCS.

After computing the EVM, the general EVM is averaged over EVM measurements for n
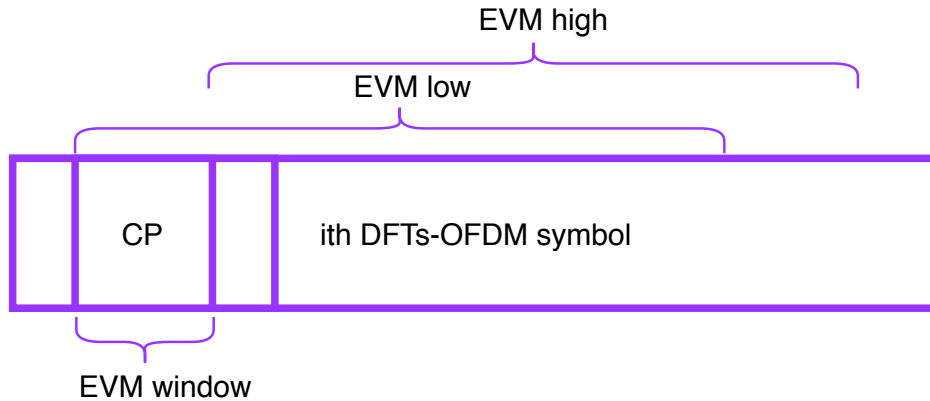
Figure 3.1. *Illustration of how to take the samples to compute EVM low and high from the received DFTs-OFDM symbol*

Table 3.1. *EVM window length for 120 kHz SCS as specified by 3GPP in TS 38.101-2*

FFT size	CP length in FFT samples	EVM window length
512	36	18
1024	72	36
2048	144	72
4096	288	144

slots in time domain (one slot comprises 14 DFTs-OFDM symbols)

$$\overline{EVM} = \sqrt{\frac{1}{n}\sum_{i=1}^{n} max(EVM_{i,l}, EVM_{i,h})^2} \qquad (3.5)$$

where

$$n = \begin{cases} 40 & if \quad \text{SCS} = 60kHz \\ 80 & if \quad \text{SCS} = 120kHz \end{cases} \qquad (3.6)$$

In this project, the EVM limits are taken from TS 38.101-2 [11] for the UE and from TS 38.104 for the BS [10]. Table 3.2 shows the EVM limits specified by 3GPP for the supported modulations in the previous mentioned documents, and these values are used as a reference in this work.

3.3 Out-of-band emission requirements

As defined in the ITU recommendation the Out-of-band (OOB) emissions are "emissions on a frequency or frequencies immediately outside the necessary bandwidth which results from the modulation process, but excluding spurious emissions" [23]. To set the limits of the OOB emissions, the 3GPP have defined emission masks and adjacent channel

Table 3.2. *EVM limits for the UE and BS according to TS 38.101-2 [11] and TS 38.104 [10]*

Modulation	EVM for UE	EVM for BS
$\pi/2$-BPSK	30 %	Not supported
QPSK	17.5 %	17.5 %
16-QAM	12.5 %	12.5 %
64-QAM	8.0 %	8.0 %
256-QAM	3.5 %	3.5 %

Table 3.3. *ACLR limits for the UE in FR2*

	Channel bandwidth / ACLR / Measurement bandwidth			
Δf_{OOB} **(MHz)**	**50 MHz**	**100 MHz**	**200 MHz**	**400 MHz**
ACLR for band n257, n258, n261	17 dB	17 dB	17 dB	17 dB
ACLR for band n260	16 dB	16 dB	16 dB	16 dB
NR channel measurement bandwidth	47.52 MHz	95.04 MHz	190.08 MHz	380.16 MHz
Adjacent channel centre frequency offset (MHz)	±50 MHz	±100 MHz	±200 MHz	±400 MHz

leakage power ratio values. In this project the spectrum mask of the 2.16 GHz channel bandwidth defined in IEEE 802.11ad is used as a reference because is a system using the frequency bands of interest for this work and the specifications are already in use (3GPP has not defined the spectrum mask for communications beyond 52.6 GHz at the time of writing this Thesis). That means that the numerology used is 180 physical resource Blocks (PRB), where 1 PRB consists of 12 subcarriers (SC) with 960 kHz subcarrier spacing (SCS).

3.3.1 ACLR limits for UE and BS

Adjacent channel leakage power ratio (ACLR) is "the ratio of filtered mean power centred on the assigned channel frequency to the filtered mean power centred on an adjacent channel frequency", as defined in [10].

The ACLR limits for the UE in FR2 are set in [11]. From that document, Table 3.3 is obtained and it shows the ACLR limits for different channel bandwidths in FR2 for the UE.

For the BS, the ACLR limits are set in [10], in this case we look at the specifications for the BS defined for FR2. Table 3.4 summarises the ACLR limits for the BS.

As reference points for this project, the ACLR limits that are considered are the most restrictive for each case, this is, 17 dB for the UE and 28 dB for the BS.

Table 3.4. *ACLR limits for the BS type 2-O in FR2 [10]*

BS channel BW	BS adjacent channel frequency offset	Assumed adjacent channel carrier	ACLR limit (dB)
50, 100, 200, 400 MHz	$BW_{channel}$	NR of same BW	28 for range 24.25-33.4 GHz 26 for range 37-52.6 GHz

However, seeing the evolution of the ACLR limits in the specifications for FR1, for example in [24], where the specifications for the UE in FR1 are defined, it is clear that when the frequency is higher, the ACLR limits are relaxed. Therefore, it could be normal to expect that the ACLR limits for frequency ranges above 52.6 GHz will be even more relaxed, so more emphasis on the UE requirements is given.

3.4   Link level performance

To evaluate the performance of the different modulations, link level performance simulations have been done. The basic metrics for the link performance evaluation are the uncoded bit error rate (BER), and the block error rate (BLER), defined as the ratio between correctly detected coded blocks and the total number of coded blocks sent. The coded performance is tested by using a 5G NR compliant link simulator. For these comparisons, the bits are encoded with a low-density parity-check (LDPC) code following 5G NR specifications [25], with different coding rates.

The first link level simulations are only under Aditive White Gaussian Noise (AWGN) channel. After the AWGN simulations, the PN is added for further comparison (the PN affects in a different way depending on the SCS and the carrier frequency). Finally, for the coded performance, a multipath channel is used to test the robustness of the modulations under a more realistic channel.

3.5   PA and PN models

In order to perform more practical evaluations, a Power Amplifier (PA) model and a Phase Noise (PN) model are needed. In this project, the PA model selected is the one defined for the IEEE 802.11ad, and the PN model is taken from the 3GPP specifications (more concretely from the TR 38.803 document [9]).

Table 3.5. *PA model parameters*

Parameter	Value
g	4.65
s	0.81
A_{sat}	0.58
α	2560
β	0.114
$q1$	2.4
$q2$	2.3

3.5.1 PA model

The PA model taken from the IEEE 802.11ad evaluation and methodology document [26] is a modified Rapp model, that generates the AM-AM and AM-PM distortion to the signal.

The AM-AM distortion has the following expression

$$G(A) = \frac{gA}{\left(1 + \left(\frac{gA}{A_{sat}}\right)^{2s}\right)^{\frac{1}{2s}}} \tag{3.7}$$

The output is given in root mean square (RMS) volts, and g is the small signal gain, s is the smoothness factor, A_{sat} is the saturation level and A is the amplitude value of the input sample.

The AM-PM distortion is defined as

$$\psi(A) = \frac{\alpha A^{q_1}}{\left(1 + \left(\frac{A}{\beta}\right)^{q_2}\right)} \tag{3.8}$$

The output is given in degrees.

The parameters used for the PA model are shown in Table 3.5, and in Figure 3.2, the AM-AM and AM-PM distortion curves can be seen against the input power.

The reference point to calculate the Input Back Off (IBO) is the 1 dB compression point, which using this model corresponds to an input power of 3.4 dBm.
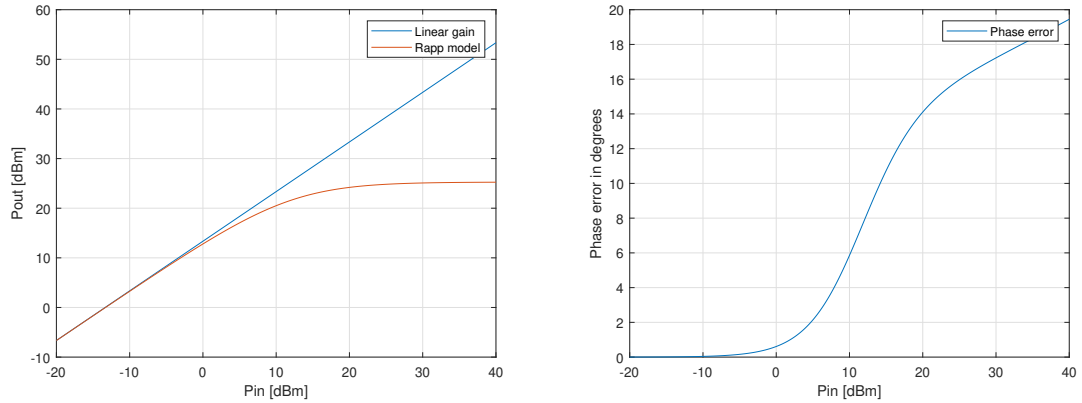
(a) Input power vs output power with the AM-AM distortion (assuming a load of 1Ω) *(b)* Input power vs phase error with the AM-PM distortion

Figure 3.2. AM-AM and AM-PM characteristic of the modified Rapp model (assuming a load of 1Ω)

3.5.2 PN model

The PN model used in this project is defined in [9]. It is a phase-locked loop (PLL)-based phase noise model. The PSD of the PN has the following expression

$$S_{total}(f) = \begin{cases} S_{ref}(f) + S_{PLL}(f) & when f \leq loopBW \\ S_{VCO_v2}(f) + S_{VCO_v3}(f) & when f > loopBW \end{cases} \tag{3.9}$$

and

$$S_{Ref/PLL/VCO_v2/VCO_v3} = PSD0 \cdot \left[\frac{1 + (\frac{f}{f_z})^k}{1 + f^k} \right] dB \tag{3.10}$$

$$PSD0 = FOM + 20 \cdot log(f_c) - 10 \cdot log \left(\frac{P}{1mW} \right) dB \tag{3.11}$$

where FOM is the figure of merit, f_c is the carrier frequency and P is the power. In the document, a different model for the UE (CMOS-based) and the BS (GaAs-based) are defined. The parameters for the models are listed in Table 3.6.

A PSD example of the PN with the UE parameters and a carrier frequency of 60 GHz is shown in Figure 3.3.

Table 3.6. *Parameters of the Phase Noise model*

	Model 1, UE, loop BW = 187 kHz				Model 2, BS, Loop BW = 112 kHz			
	REF clk	**PLL**	**VCO v2**	**VCO v3**	**REF clk**	**PLL**	**VCO v2**	**VCO v3**
FOM	-215	-240	-175	-130	-240	-245	-187	-130
f_z	Inf	1.00E+04	50.30E+06	Inf	Inf	1.00E+04	8.00E+06	Inf
P (mW)	10	20	20	20	10	20	50	50
k	2	1	2	3	2	1	2	3
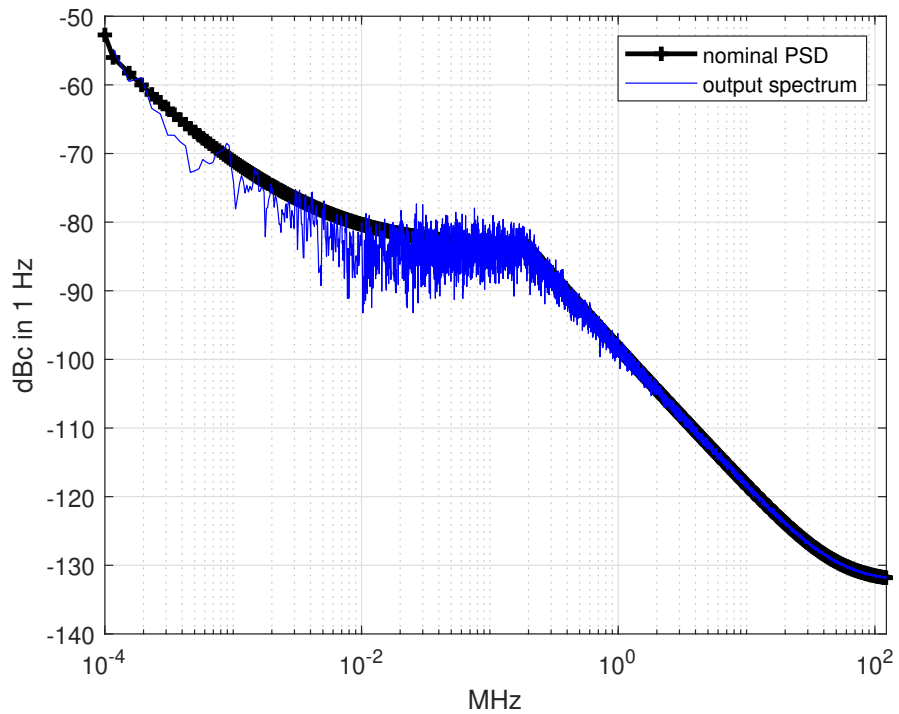
Figure 3.3. *PSD of the PN with the UE parameters and carrier frequency of 60 GHz [9]*

4 TECHNIQUES TO REDUCE PAPR

In this chapter, some techniques that have been used to reduce the PAPR of the signal are presented and explained. There are three main techniques: root raised cosine (RRC) filtering, π/M rotation and spectral shapping.

4.1 RRC filtering

According to [27], the roll-off factor of the RRC filter influences the PAPR of the signal. Up to some value of roll-off, which in this thesis is typically around 0.5-0.6, the PAPR of the signal can be improved.

In the case of DFTs-OFDM, the best way to apply the RRC filter is to implement it in the frequency domain and use it as a pulse shaping filter between the FFT and the IFFT, by means of frequency domain processing. The process of filtering is illustrated in Figure 4.1. After the M point DFT is performed, the frequency domain samples have to be cyclically extended up to Q ($Q = M(1 + \alpha)$ where α is the roll-off factor). This in fact, reduces the spectral efficiency (SE) of the signal since it means that more SC are used for the transmission. After the cyclic extension is done, the Q samples are multiplied by the frequency domain coefficients of the RRC filter, so the complexity of the transmitter does not increase much.

The RRC filter in frequency has the following expression

$$H(f) = \begin{cases} \sqrt{T} & if \quad 0 < |f| \leq \frac{1-\alpha}{2T} \\[2em] \sqrt{\frac{T}{2}(1 + cos(\frac{\pi T}{\alpha}(|f| - \frac{1-\alpha}{2T})))} & if \quad \frac{1-\alpha}{2T} \leq |f| \leq \frac{1+\alpha}{2T} \\[2em] 0 & if \quad |f| \leq \frac{1+\alpha}{2T} \end{cases} \tag{4.1}$$

Figure 4.2 illustrates some examples of RRC filters in frequency with different roll-off factors are shown (all the RRC filters are normalised to unit power and use 180 PRBs, thus modelling the case where less information bits are sent when the roll-off increases, but always the same bandwidth is used).

For example, for the $\pi/4$-QPSK (modulation explained in chapter 5), using RRC filtering,
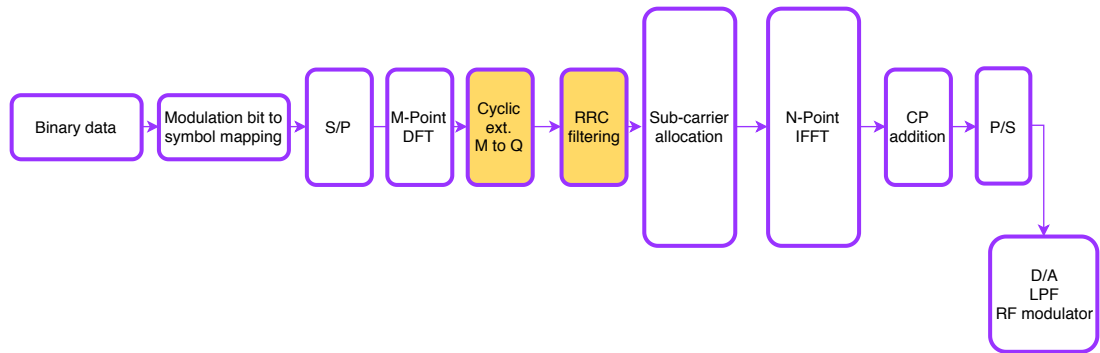
Figure 4.1. *DFTs-OFDM modulator including RRC filtering in frequency*
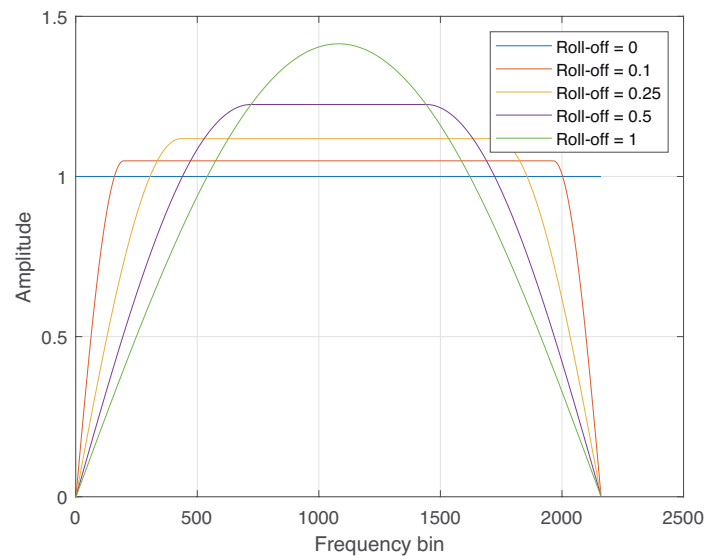
Figure 4.2. *RRC filters in frequency domain for different roll-off factors*

the PAPR can be reduced from 4.5 dB at 1% probability point of the CCDF when no RRC filter is used, down to 2.4 dB using a roll-off of 0.5. Once the roll-off goes higher than 0.5, the PAPR value starts to increase (see Figure 4.3).

4.2 π/M **rotation**

The π/M (where M is the order of the modulation in case of PSK modulations, or $M = 2$ with PAM modulation) rotation is applied in time for all the symbols. It is done in order to avoid the 180º of phase shift between two consecutive symbols. By doing this, the PAPR of the signal can be considerably reduced.

This phase rotation can be easily applied in the digital domain after performing the bit to symbol mapping. As explained before, if $M = 2$ for BPSK, assuming that $\tilde{s}_k$ is the kth symbol to be sent, the phase shift to apply to that symbol is $e^{j\pi\frac{k}{2}}$ or $e^{j\pi\frac{mod(k,2)}{2}}$. This way, for BPSK, the maximum phase transition between consecutive symbols is 90º ($\pi/2$ radians). Equation (4.2) shows the mathematical expression to be performed over the
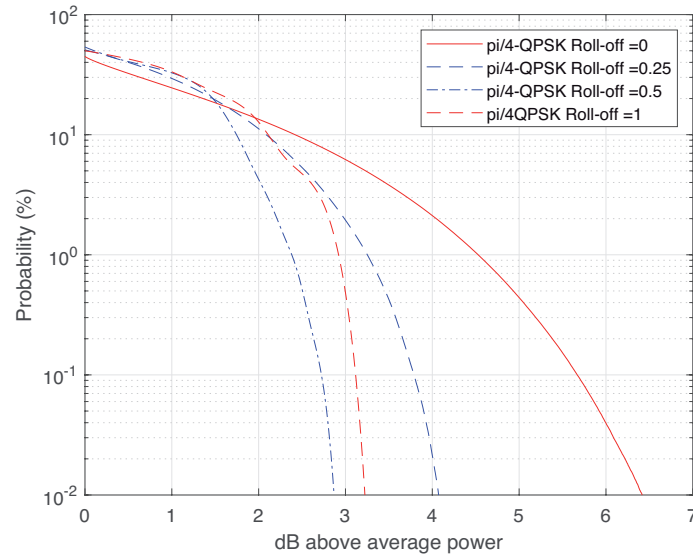
Figure 4.3. *Example of PAPR distributions for $\pi/4$-QPSK using different roll-off factors.*
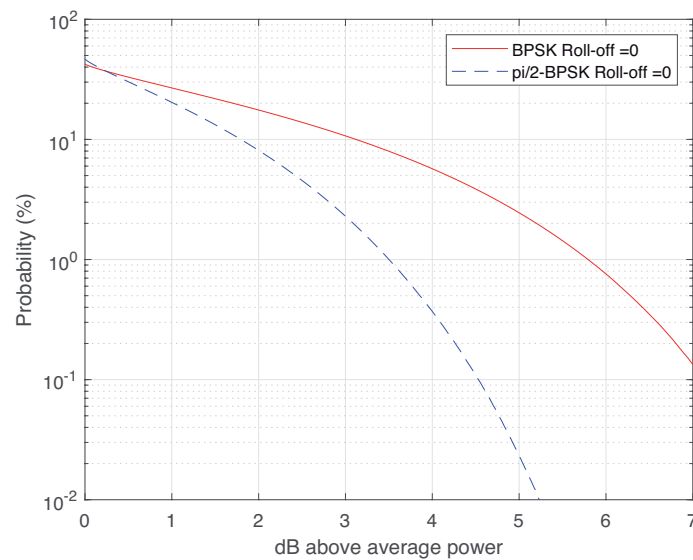
Figure 4.4. *Example of PAPR distributions comparing BPSK and $pi/2$-BPSK.*

kth symbol.

$$s_k = \tilde{s}_k e^{j\pi \frac{k}{2}} \tag{4.2}$$

Figure 4.4 shows the reduction in PAPR that can be obtained for BPSK (modulation explained in chapter 5) if the $\pi/2$ rotation is applied (from 5.8 dB down to 3.5 dB).
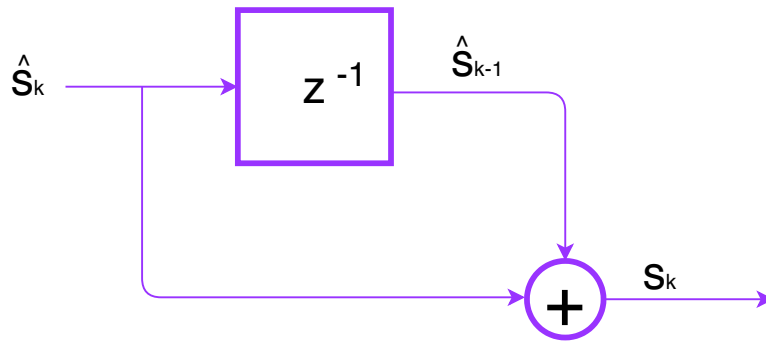
Figure 4.5. *Block dagram of the [1-D] filter*
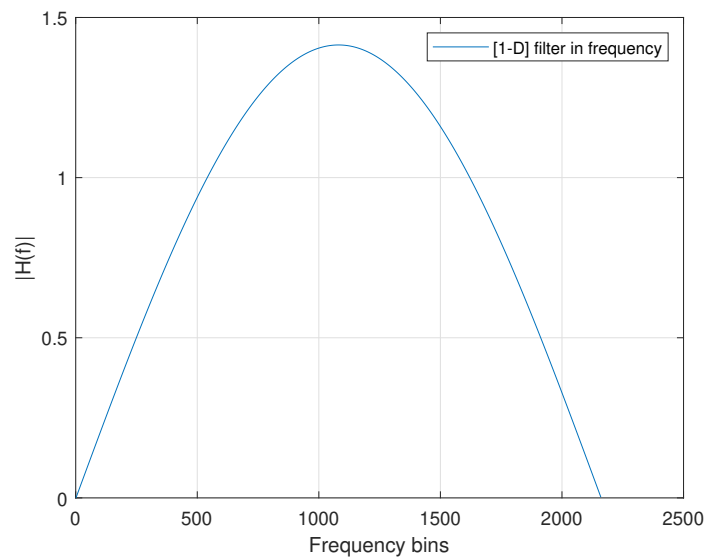
Figure 4.6. *[1-D] filter in frequency*

4.3 Spectral shaping

The spectral shaping applied in this study consists on a precoder applied in time to the symbols without oversampling [28]. The precoder is a 2-tap filter denoted as [1-D], where D represents delay of one symbol. Figure 4.5 shows the block diagram of the [1-D] filter, where $\hat{s}_k$ and $\hat{s}_{k-1}$ are the kth and $(k-1)$th symbols, one of them is in the real axis and the other is in the imaginary axis. The [1-D] spectral shaping filter is here assumed to be applied after performing the $\pi/2$ rotation to the symbols belonging to a real constellation (such as BPSK or 4PAM).

After the filter is applied, the new constellation have memory, for example in the case of [1-D]$\pi/2$-BPSK (modulation explained in chapter 5), the obtained constellation is like a QPSK with memory. The frequency response of the [1-D] filter is shown in Figure 4.6 (using 2160 subcarriers), it looks like an RRC filter of roll-off factor of 1, but in this case there are no losses in spectral efficiency.

After applying the spectral shaping filter, the PAPR of the signal can be even further reduced. Figure 4.7 shows the example of the PAPR reduction for the [1-D]$\pi/2$-BPSK,
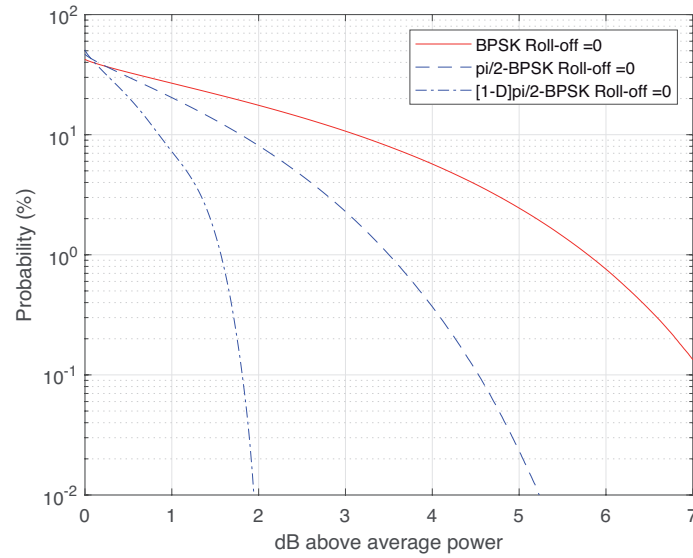
Figure 4.7. *Example of the PAPR distribution of [1-D]$\pi/2$-BPSK vs $\pi/2$-BPSK vs $\pi/2$-BPSK*

down to 1.5 dB. This modulation is state-of-the-art and provides the best trade-off in terms of complexity against performance when targeting very low PAPR waveforms with low spectral efficiency, and therefore is another important reference in addition to QPSK.

5 STUDIED MODULATIONS

5.1 Reference modulations

In this project, we are targeting specially low spectral efficiency moduations and for that reason, the modulations used for comparison vary from 1 bit per symbol to 2 bits per symbol. With 1 bit per symbol, the modulation studied is the BPSK and different variants that are going to be explained in this chapter and with 2 bits per symbol, the main reference modulations are QPSK (and its variants) and the 4PAM (and its variants). Also, as a main contribution from this project, a modulation that uses constrained mapping to assign bits to symbols, and that achieve a spectral efficiency of 1.5 bps/Hz or 2 bps/Hz is studied. The proposed modulation is denoted as Constrained PSK (CPSK).

5.1.1 BPSK, $\pi/2$-BPSK and [1-D]$\pi/2$-BPSK

BPSK

Binary phase shift keying (BPSK) is a well known digital modulation that carries one bit per symbol and transmits symbols using two different phases with 180º separation. In the special case that these phases are 0º and 180º, this modulation corresponds to 2PAM modulation, and the information can be considered to be carried only by the real-part of the signal. The constellation of this modulation is shown in Figure 5.1. The bit to symbol mapping is very simple, starting from the set of bits (c_k = 0 or 1), the symbol s_k is obtained as

$$s_k = a_k e^{j\theta_k} \tag{5.1}$$

where $\theta_k = \pi c_k$ and $a_k = 1$. Resulting in

$$s_k^{BPSK} = e^{j\pi c_k} \tag{5.2}$$

$\pi/2$-BPSK

$\pi/2$-BPSK is a modification of the basic BPSK. The difference is that every symbol, there is a 90º ($\pi/2$ rad) rotation. This way, between 2 consecutive symbols, the zero crossing
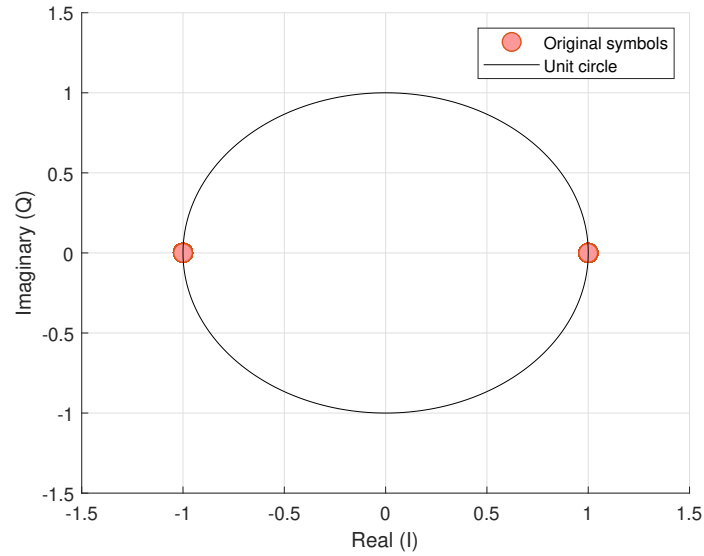
Figure 5.1. *BPSK constellation*
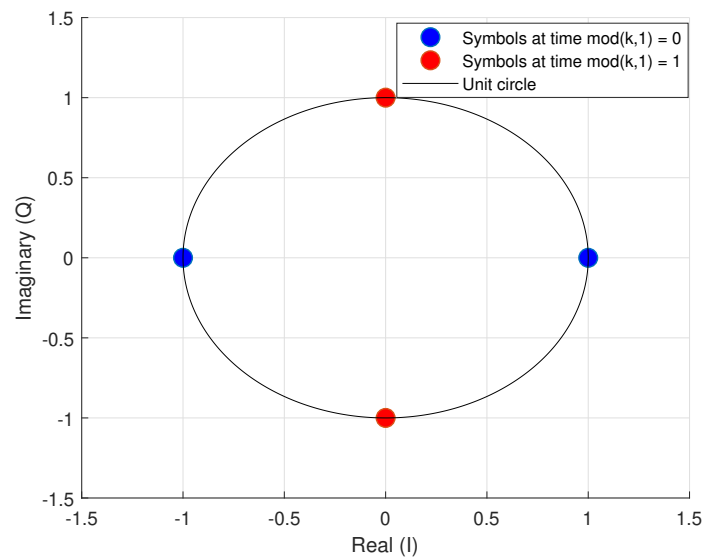
Figure 5.2. $\pi/2$-*BPSK constellation*

is avoided and the PAPR is reduced. The bit to symbol mapping is as follows

$$s_k^{\pi/2-BPSK} = s_k^{BPSK} e^{j\pi \frac{k}{2}} \tag{5.3}$$

Since there is a 90º rotation each symbol, the full constellation presents 4 symbols. However, for each symbol time instant, the data is transmitted either in the real (blue symbols in Figure 5.2, for even symbol index, k) or in the imaginary dimension (red symbols in Figure 5.2, for odd symbol index, k).
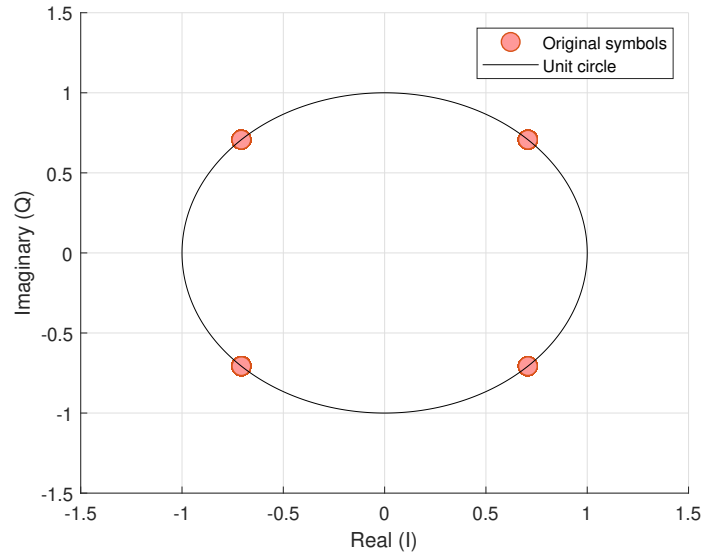
Figure 5.3. *[1-D]$\pi/2$-BPSK constellation*

[1-D]$\pi/2$-BPSK

[1-D]$\pi/2$-BPSK is a further modification of the previous explained modulation. The [1-D] term means that a spectral shaping is performed over 2 consecutive symbols (the current and previous one). The delay D corresponds to a delay of one symbol duration. It is called spectral shaping because it changes the spectral shape of the signal and it can be seen as an RRC type spectrum after applying the filter (see Section 4.3 for further explanation).

The bit to symbol mapping is the same as for the $\pi/2$-BPSK and after that, the combination is done, and can be defined as

$$s_k^{[1-D]\pi/2-BPSK} = \frac{s_k^{\pi/2-BPSK} + s_{k-1}^{\pi/2-BPSK}}{\sqrt{2}} \tag{5.4}$$

The $k-1$ operation is done applying the module of the length of the block of symbols encoded in the case of DFTs-OFDM.

The constellation now is rotated 45º since a real symbol is combined with an imaginary symbol (see Figure 5.3). However, the information bearing signal is still only in one domain, and the signal component in the other domain can be considered as inter-symbol-interference (ISI). Because the information bearing signal and ISI are in different domains, their separation is straightforward in the receiver.

(a) QPSK constellation

(b) $\pi/4$-QPSK constellation
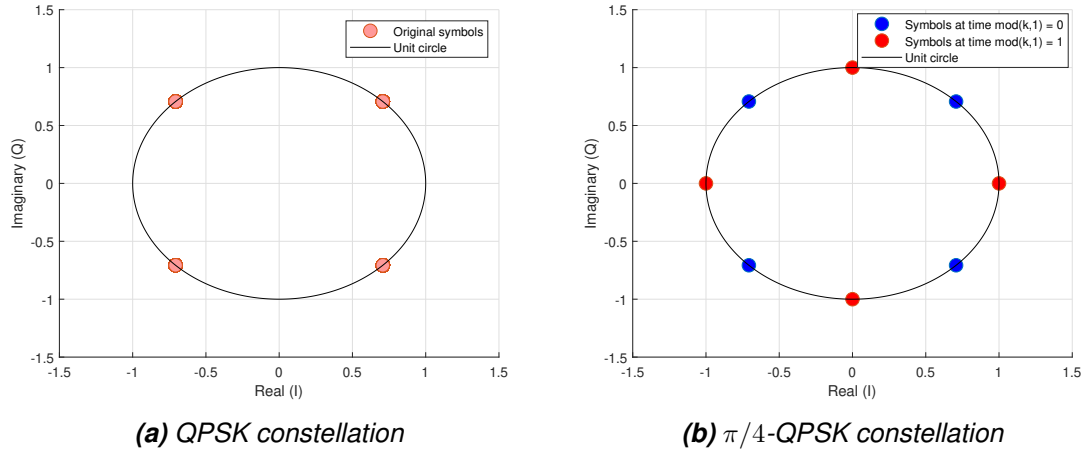
Figure 5.4. QPSK and $\pi/4$-QPSK constellations

5.1.2 QPSK and π/4-QPSK

QPSK

QPSK is a well known digital modulation that has 4 symbols, each carrying 2 bits. The phases of the symbols are usually 45º, 135º, 225º and 315º. The mapping from bits to symbols is

$$s_k = \frac{1}{\sqrt{2}} \left[(2c_{2k} - 1) + j(2c_{2k+1} - 1) \right] \tag{5.5}$$

Where c_k is the k bit. The obtained constellation is shown in the Figure 5.4a.

$\pi/4$-QPSK

$\pi/4$-QPSK is a modification of the basic QPSK. Every symbol time, the constellation is rotated 45º ($\pi/4$ rad) in order to avoid zero crossing or 180º phase change (same principle as the $\pi/2$ rotation for BPSK). In one symbol time instant, the information is sent in the constellation [45º, 135º, 225º, 315º] and in the next one in [0º, 90º, 180º, 270º].

The bit to symbol mapping is as follows (the constellation is shown in the Figure 5.4b)

$$\tilde{s}_k = \frac{1}{\sqrt{2}} \left[(2c_{2k} - 1) + j(2c_{2k+1} - 1) \right]$$
$$s_k = \tilde{s}_k e^{j\pi \frac{k}{4}} \tag{5.6}$$
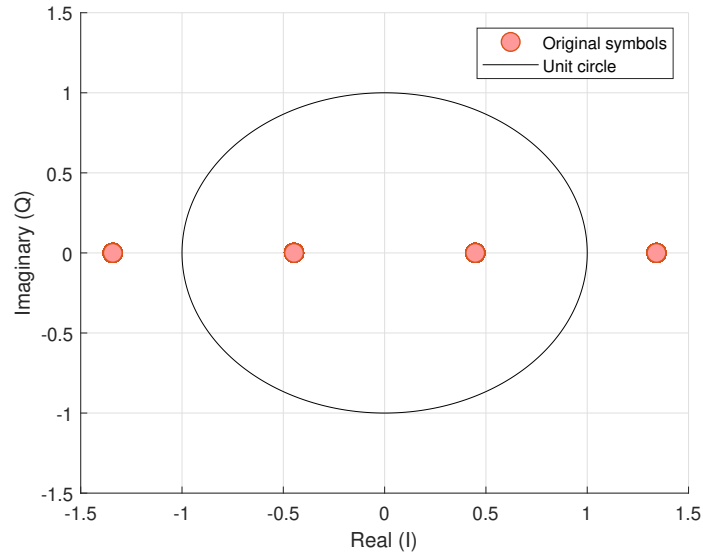
Figure 5.5. *4PAM constellation*

5.1.3 4PAM

4PAM is a digital pulse amplitude modulation where 4 different amplitudes are used to transmit the data. Each symbol carries 2 bits. The phase of the symbols remains constant between different symbols since 4PAM has a real constellation. The bits to symbol mapping is as follows

$$s_k = \frac{1}{\sqrt{5}} \left(2m - 1 - 4\right) \tag{5.7}$$

where m is the decimal representation of the 2 bits c_{2k} and c_{2k+1}. The constellation is shown in the Figure 5.5.

5.2 Proposed modulations

In this section, the modulations that are not used in current communication systems or have not been found on the related literature, and have been studied in this work are presented.

5.2.1 $\pi/2$-4PAM and [1-D]$\pi/2$-4PAM

$\pi/2$-4PAM

This modulation is a modification of the previously explained 4PAM. The difference is now that every symbol, the constellation is rotated 90º ($\pi/2$ rad) in order to make the phase difference between 2 consecutive symbols 90º and not 180º as it is for normal 4PAM.
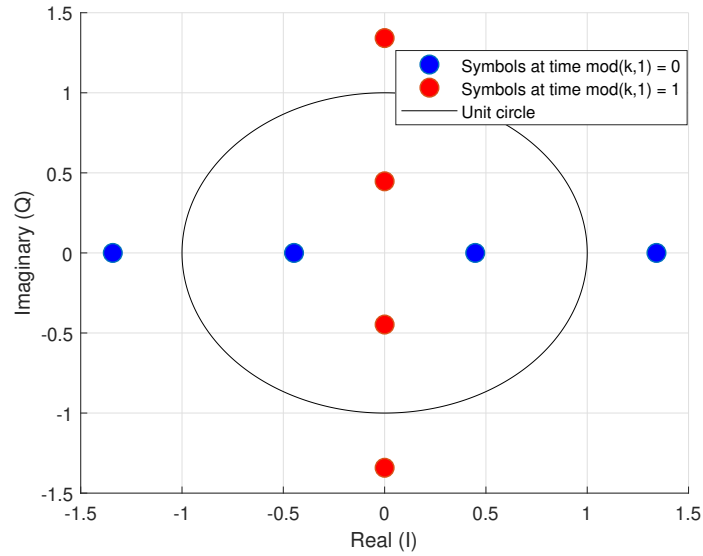
Figure 5.6. *$\pi/2$-4PAM constellation*

The mapping from bits to symbols is expressed as

$$\tilde{s}_k = \frac{1}{\sqrt{5}}\left(2m - 1 - 4\right)$$
$$s_k = \tilde{s}_k e^{j\pi\frac{k}{2}}$$

(5.8)

As it was for the $\pi/2$-BPSK, every other symbol is transmitted in the real domain and every other in imaginary domain.

[1-D]$\pi/2$-4PAM

The [1-D]$\pi/2$-4PAM is again, as in the case of [1-D]$\pi/2$-BPSK, the spectral shaped version of $\pi/2$-4PAM. Two consecutive symbols are combined, and the bit to symbol mapping is done as follows

$$\tilde{s}_k = \frac{1}{\sqrt{5}}(2m - 1 - 4)$$
$$\hat{s}_k = \tilde{s}_k e^{j\pi\frac{k}{2}}$$
$$s_k = \frac{\hat{s}_k + \hat{s}_{k-1}}{\sqrt{2}}$$

(5.9)

The resulting constellation has 16 points since they are the combination of a real symbol with an imaginary symbol (see Figue 5.7).
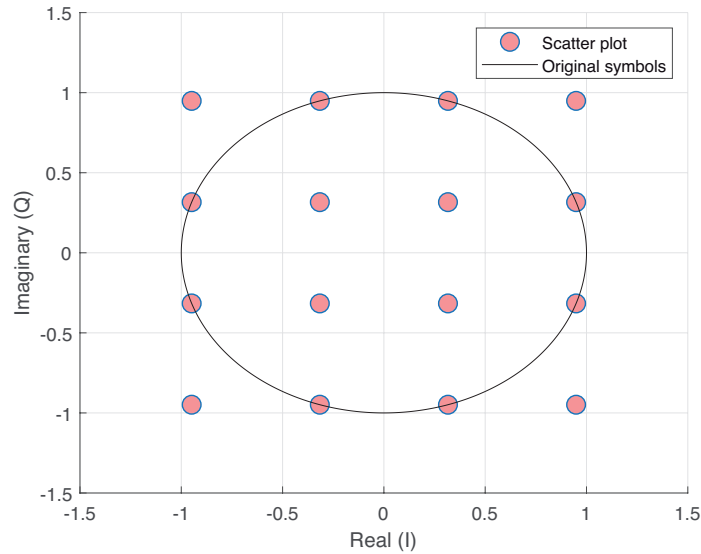
Figure 5.7. *[1-D]$\pi/2$-4PAM constellation*

5.2.2 Constrained PSK

The Constrained PSK (CPSK) modulation is a new proposal with the main goal of reducing the PAPR of the signal when compared to QPSK modulation. They are based on PSK constellations of sizes from 4 to 8 symbols, where the symbols are placed in the unit circle and with a phase of $\frac{2\pi}{M}k$ for the symbol k of the constellation, and M is the number of symbols.

The constraint is applied in time domain to the assigned symbols depending on the input bits, and since the objective is to reduce the PAPR, the transitions between symbols in the scatterplot diagram avoid the zero-crossing and try to stay close to the unit circle. In this Thesis, two possible constraints are studied. Starting from a symbol of the constellation, one constraint allows 3 possible options (noted as CMPSK/3) for the next symbol to sent, and the second constraint allows 4 possible options (noted as CMPSK/4) for the next symbol. The constraint with 3 options carries 1.5 bits per symbol sent and the constraint with 4 options carries 2 bits per symbol sent.

The constraint can be applied in groups of bits to form CPSK blocks, and after each block has been mapped to symbols, the first symbol of the next block can be freely chosen, from where the constraint is applied to the remaining bits of the block. By doing this, all the blocks can be decoded in parallel, thus reducing the receiver processing time. Examples of bit to symbol mapping tables for all the studied modulations and constraints are shown in the Appendix A.

Let us look at an example of the C5PSK/3 modulation, where the constraint allows 3 possible symbols (see Figure 5.8, where the last symbol sent was s_1, therefore the next possible symbol is indicated by the arrows and it can be either s_0, s_1 or s_2). Since there are 5 possible symbols in the C5PSK modulation, there are 5 columns in the table (one
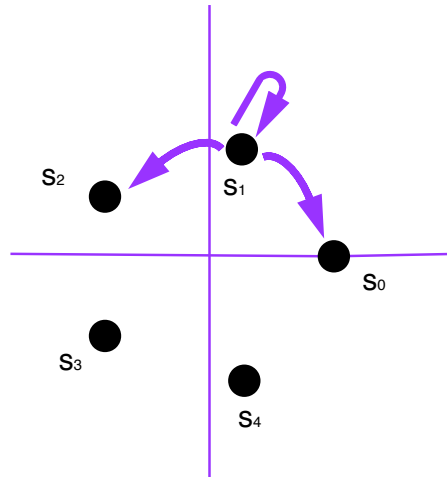
Figure 5.8. *C5PSK/3 constellation. Example from symbol s_1*

Table 5.1. *Bit to symbol mapping example for C5PSK/3*

Input bits	Previous symbol									
	s_0		s_1		s_2		s_3		s_4	
000	s_0	s_1	s_1	s_2	s_2	s_3	s_3	s_4	s_4	s_0
001	s_0	s_4	s_1	s_0	s_2	s_1	s_3	s_2	s_4	s_3
010	s_1	s_2	s_2	s_3	s_3	s_4	s_4	s_0	s_0	s_1
011	s_4	s_3	s_0	s_4	s_1	s_0	s_2	s_1	s_3	s_2
100	s_1	s_0	s_2	s_1	s_3	s_2	s_4	s_3	s_0	s_4
101	s_4	s_0	s_0	s_1	s_1	s_2	s_2	s_3	s_3	s_4
110	s_1	s_1	s_2	s_2	s_3	s_3	s_4	s_4	s_0	s_0
111	s_4	s_4	s_0	s_0	s_1	s_1	s_2	s_2	s_3	s_3

for each previous symbol), see Table 5.1.

In the case of 3 possible symbols per symbol time instant, 2 symbols are needed to carry 3 bits, therefore resulting on a spectral efficiency of 1.5 bps/Hz. The mapping works as follows (see Table 5.1 for reference):

1. Input bits are divided in N blocks of $3K$ bits.

2. Based on the CPSK block index (i_{CPSK}), the column $mod(i_{CPSK}, M)$ of the set of tables is used.

3. The value of the 3 bits (between 0 and 7) gives the index of the row in the table that contains the pair of symbols to be sent and that follow the constraint.

4. The second symbol selected from the table at step 3 defines the next column to use (i.e., if the second symbol of the pair is s_2, the next column to use will be the column below s_2).

5. Repeat steps 3 and 4 until all the bits of the block i_{CPSK} are mapped.

In the case of 4 options, the bit to symbol mapping is different. Also, like for the previous

Table 5.2. Bit to symbol mapping example for C5PSK/4. Even/odd symbol index

Input bits	Previous symbol				
	s_0	s_1	s_2	s_3	s_4
00	s_0	s_1	s_2	s_3	s_4
01	s_1	s_2	s_3	s_4	s_0
10	s_4	s_0	s_1	s_2	s_3
11	s_2/s_3	s_3/s_4	s_4/s_0	s_0/s_1	s_1/s_2

case, the constraint can be applied in blocks. Since the constraint allows 4 possible symbols for each input, the bits inside the block are taken in pairs. Some things have to be taken into consideration for the 4 possibilities constraint, one is that since there are 4 options every symbol, the transitions are not symmetric and they generate frequency components that have to be avoided, therefore to combat this, the mapping tables are different for the even symbol index and for odd symbol index.

Since there are 4 possibilities per time instant, 1 symbol is needed to carry 2 bits, therefore the spectral efficiency of the 4 options case is 2 bps/Hz. The bit to symbol mapping works as follows (see Table 5.2 for reference):

1. Divide the input bits in N blocks of $2K$ bits.

2. Based on the CPSK block index (i_{CPSK}), the column $mod(i_{CPSK}, M)$ of the set table is used.

3. Two bits are taken, and the symbol to be sent is the one on the row that corresponds to the pair of bits in the column chosen at the previous step, for even symbol index. The sent symbol gives the next column to be used.

4. Two bits are taken, and the symbol to be sent is the one on the row that corresponds to the pair of bits in the column chosen at the previous step, for odd symbol index. The sent symbol gives the next column to be used.

5. Repeat steps 3 and 4 until all the bits of the block i_{CPSK} are mapped.

For example, for the column s_2 (this means that the previous symbol sent has been s_2), the next output symbol would be s_2 if the input bits are "00", s_3 if the input bits are "01" and s_1 if the input bits are "10". For the even symbol index when the input bits are "11", the output would be s_0 whereas for the odd symbol index the output would be s_4 (note that this mapping is just to exemplify. The bit to symbol mapping can be changed independently of the base constellation or the constraint applied in order to improve the BER performance or maximize the Euclidean distance between symbols carrying similar bits, for example). The even and odd mapping tables for C5PSK/4 are shown in Table 5.2.

For further reduce the PAPR of the signal in the 4 options case, a base constellation rotation of π/M radians every other symbol makes the iPAPR decrease considerably, without affecting the detection performance. Therefore, after the bit to symbol mapping is performed, a phase rotation of the form $e^{j\pi mod(k,2)/M}$ can be applied, where k is the
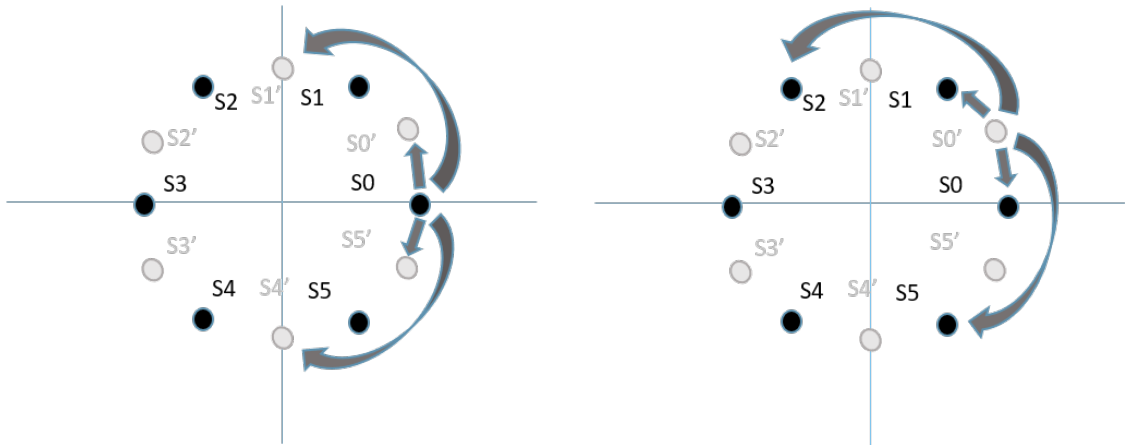
Figure 5.9. *Example transitions for C6PSK/4 modulation with base constellation rotation every other time instant*
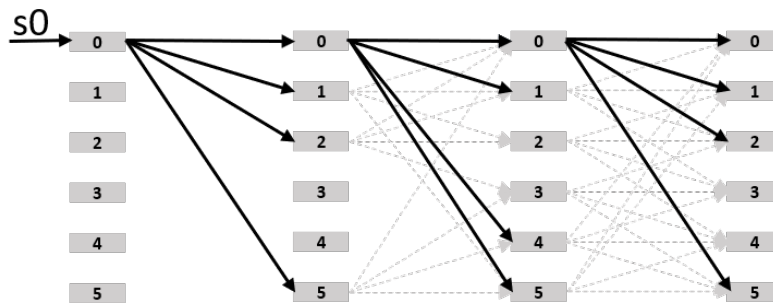
Figure 5.10. *Example trellis of C6PSK/4 modulation*

symbol index. The resultant transitions are illustrated in Figure 5.9 for the C6PSK/4 case (the black symbols are used for even symbol index and the grey are the rotated constellation used for the odd symbol index).

To decode the bits at the receiver, it can be done by means of a Viterbi or BCJR [29] algorithm, if the receiver incorporates memory. As another possibility when the memory is not used, the bit to symbol mapping could be also defined in such a way that the receiver utilises a plain PSK detector assuming a PSK constellation with M symbols, therefore decreasing the complexity at the receiver side.

For example, for the 4 options case, the Trellis diagram evolution for C6PSK/4 is illustrated in Figure 5.10, where the first transmitted symbol is assumed to be s_0 and the transitions from state 0 are highlighted to note the difference between the even and odd symbol index.

As an example to illustrate the transmitted DFTs-OFDM signals with CPSK modulations, the IQ scatterplot diagrams of C6PSK/4 with rotation (note the double number of symbols due to even and odd constellations) and C6PSK/3 are shown in Figure 5.11. As a comparison to show the characteristics of the new proposed CPSK modulations, Figure 5.12 illustrates the IQ scatterplot for DFTs-OFDM signals with [1-D]$\pi/2$-BPSK and QPSK modulations. It can be seen that for the QPSK, there are several zero crossings, which
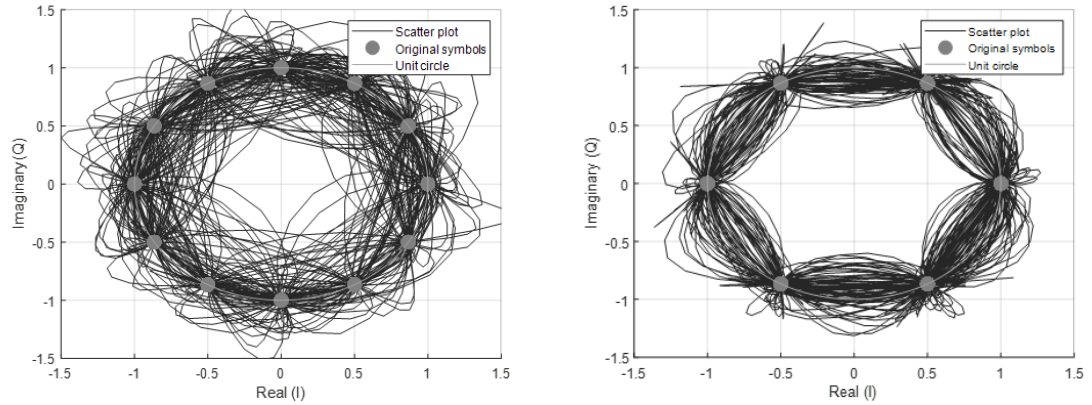
(a) *IQ scatterplot of the transmitted signal with C6PSK/3 modulation*

(b) *IQ scatterplot of the transmitted signal with C6PSK/3 modulation*

Figure 5.11. *IQ scatterplots for C6PSK/4 and C6PSK/3*
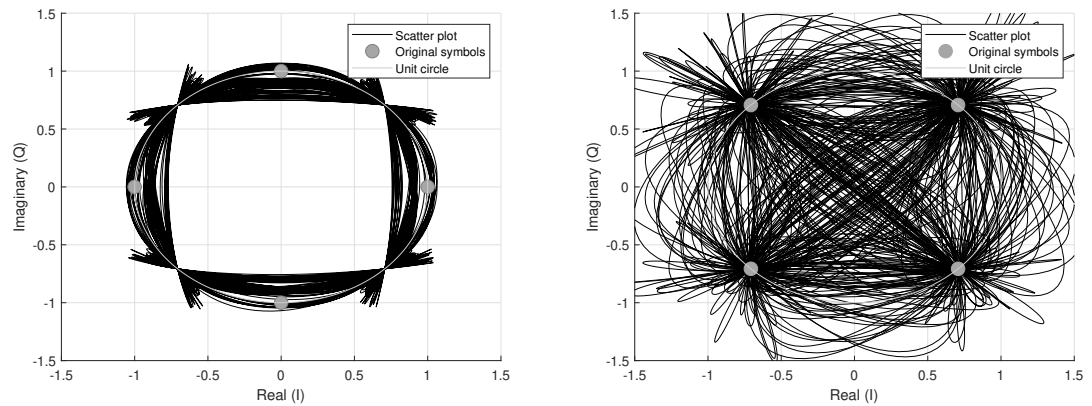
(a) *IQ scatterplot of the transmitted signal with [1-D]π/2-BPSK modulation*

(b) *IQ scatterplot of the transmitted signal with QPSK modulation*

Figure 5.12. *IQ scatterplots for [1-D]π/2-BPSK and QPSK*

means that the PAPR of the signal will be high. However, for the [1-D]π/2-BPSK, the scatterplot shows that the signal is really close to the unit circle, therefore indicating that the PAPR is low. The benefit of the CPSK modulation is that it can achieve lower PAPR than QPSK with a higher SE than [1-D]π/2-BPSK.

6 NUMERICAL RESULTS

In this chapter, the numerical results are presented. First, there is a study of the PAPR for the different modulations and waveforms. Following the PAPR study, the maximum PA output power per modulation fulfilling the OOB requirements is computed, then the link performance evaluations with AWGN are introduced. Also, the PN is added and the link performance under the effects of PN is noted. Finally, the coded link performance using a 5G NR compliant simulator is obtained.

With all the previous results, the link budget gain of the studied modulations against the reference modulation is calculated in order to select the possible candidates. In this work, the link budget gain is simply the summation of the PA output gain and link performance gain, with respect to QPSK reference waveform with roll-off = 0.

Table 6.1 shows the main physical layer parameters that have been used in order to run the simulations (when there are more than 1 value, the value selected for the simulation is noted in the text).

6.1 PAPR study

As it was explained through the different chapters of the thesis, the PAPR that the waveform presents is very important since it will determine the working point of the PA, and therefore the maximum achievable output power. For that reason, we start with a comparison the PAPR of the different modulations.

We start by comparing the PAPR of the DFTs-OFDM against the CP-OFDM, carrying the same modulation. In the 1 % probability point of the iPAPR distribution, for the QPSK modulation, the DFTs-OFDM waveform presents 4.5 dB, while the CP-OFDM has 6.6 dB (see Figure 6.1). CP-OFDM can not achieve the same PAPR than DFTs-OFDM with the same modulation order and it is not going to be taken into consideration in the continuation.

As explained in chapter 4, the RRC filtering can help to reduce the PAPR of the signals (although it degrades the spectral efficiency (SE)). For all the modulations to be compared, the PAPR distributions has been obtained for roll-off factors of 0, 0.1, 0.25, 0.5 and 1.

***Table 6.1.** Main physical layer parameters for the numerical evaluations*

Parameter	Value
Active subcarriers (M)	180 · 12 = 2160
IFFT size (N)	4096
Subcarrier spacing (SCS)	120 kHz or 960 kHz
Allocated bandwidth	259.2 MHz or 2073.6 MHz
Channel bandwidth	2160 MHz
Sampling frequency (nominal)	N · SCS = 491.52 MHz or 3.93 GHz
Oversampling factor (osf)	4
Sampling frequency (used in PAPR evaluations)	N · SCS · osf = 1.96 GHz or 15.72 GHz
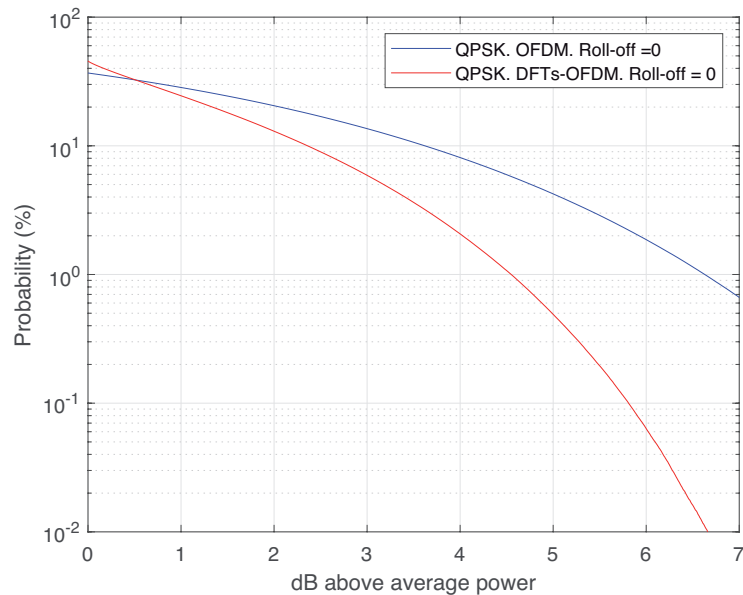
***Figure 6.1.** Comparison of the iPAPR of OFDM and DFTs-OFDM with QPSK modulation*

6.1.1 $[1 - D]\pi/2$-**BPSK**

For the $[1 - D]\pi/2$-BPSK modulation, in the Figure 6.2, the CCDF distributions of the iPAPR and PAPR per DFTs-OFDM symbol are shown. From that figure, it can be seen that increasing the roll-off does not improve the PAPR of the signal. This is because the time domain filtering with [1-D] effectively applies an RRC filter with roll-off = 1 to the signal. The waveform with smaller iPAPR at 1% probability is achieved with a roll-off of 0.5, however the gain in iPAPR is just 0.05 dB while the SE drops from 1 bps/Hz down to 0.66 bps/Hz. As a consequence, for the $[1 - D]\pi/2$-BPSK modulation, only the case of roll-off 0 is going to be taken into consideration. Also worth to mention, as it has been shown, the PAPR that the $[1 - D]\pi/2$-BPSK modulation presents is smaller than for the $\pi/2$-BPSK, or the normal BPSK, thus, they are not going to be included in the comparisons.

(a) *iPAPR*

(b) *PAPR per DFTs-OFDM symbol*
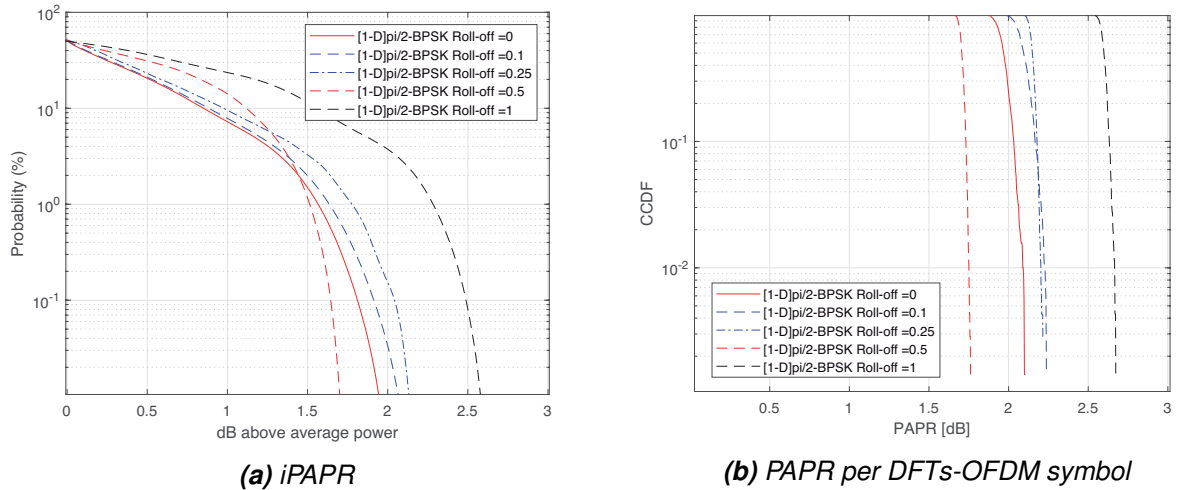
Figure 6.2. *CCDF distributions of PAPR for $[1-D]\pi/2$-BPSK with different roll-off values*
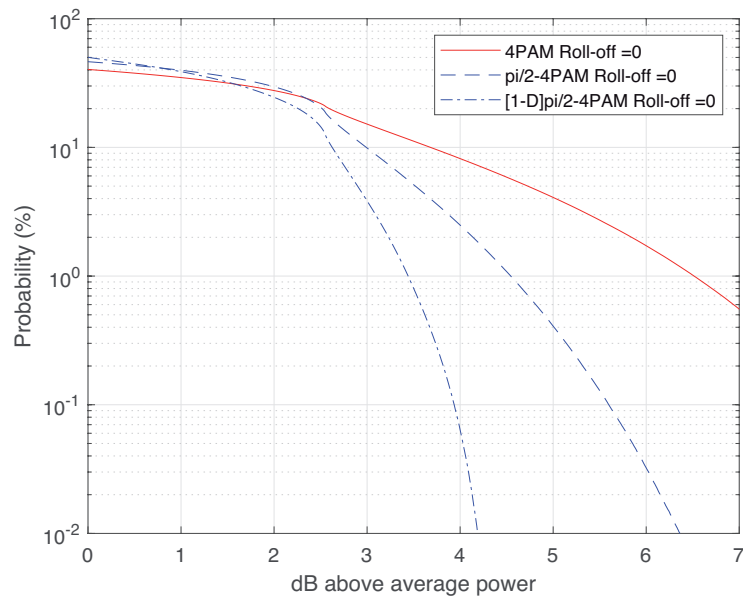
Figure 6.3. *Comparison of the iPAPR of 4PAM and its variants*

6.1.2 $[1-D]\pi/2$**-4PAM**

For the 4PAM modulations and its variants ($\pi/2$-4PAM and $[1-D]\pi/2$-4PAM), similarly to the BPSK study, we can take a look at the PAPR distributions and select one out of the three candidates. Figure 6.3 shows the iPAPR distributions. Like in the BPSK case, including the $\pi/2$ rotation and then the [1-D] spectral shaping filter, the PAPR can be reduced (from 6.50 dB down to 3.45 dB). Only the $[1-D]\pi/2$-4PAM will be taken into consideration in the continuation.

Figure 6.4 shows the PAPR distributions of the $[1-D]\pi/2$-4PAM for different roll-off values. Like for the $[1-D]\pi/2$-BPSK case, increasing the roll-off does not improve the PAPR of the signal. Hence, only the case of roll-off 0 will be studied.

(a) iPAPR

(b) PAPR per DFTs-OFDM symbol
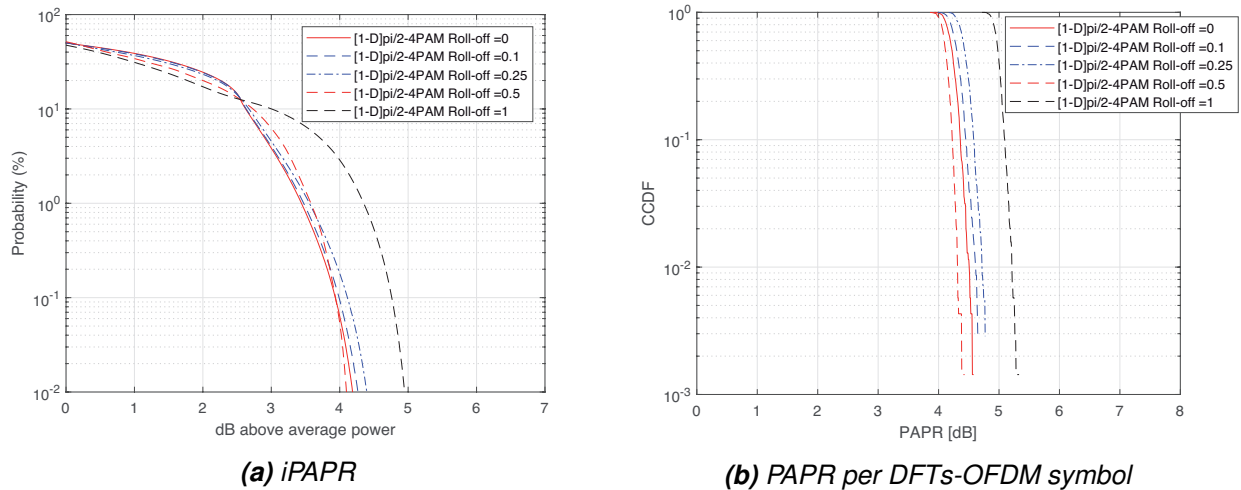
Figure 6.4. CCDF distributions of PAPR for $[1-D]\pi/2$-4PAM with different roll-off values

(a) iPAPR

(b) PAPR per DFTs-OFDM symbol
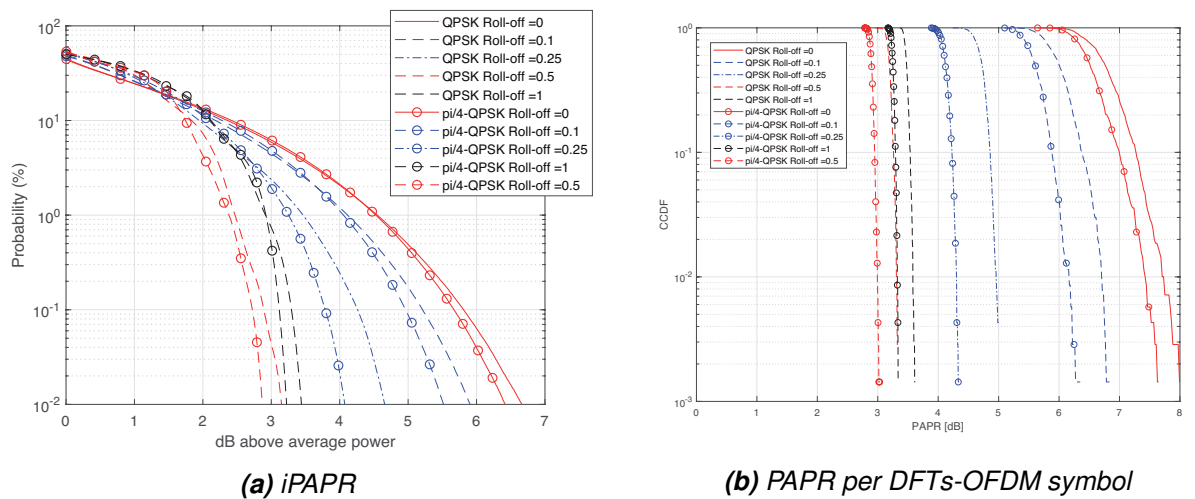
Figure 6.5. CCDF distributions of PAPR for QPSK and $\pi/4$-QPSK with different roll-off values

6.1.3 QPSK and $\pi/4$-QPSK

The next modulations to be studied are the QPSK and the $\pi/4$-QPSK. Both carry the same amount of bits per symbol. Figure 6.7 shows the PAPR distributions of the QPSK and $\pi/4$-QPSK modulation for different roll-off values. In this case, increasing the roll-off up to 0.5 helps to reduce the PAPR of the signals (if the roll-off is higher than 0.5, the PAPR starts to increase). Also, it can be seen that the $\pi/4$-QPSK presents smaller PAPR values than the basic QPSK when both have the same roll-off, and the complexity in the transmitter and receiver is the same. However, the spectral efficiency is an important factor and therefore the QPSK with roll-off = 0 will be used as a reference in the continuation since is already supported by the 3GPP specifications.
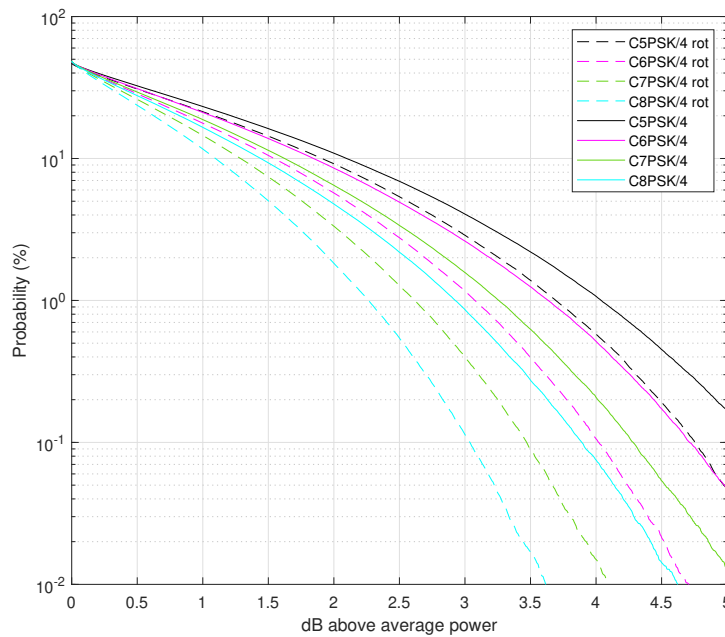
Figure 6.6. *Comparison of the iPAPR of the CPSK/4 modulations with and without rotation*

6.1.4 CPSK

For the CPSK modulations, Figure 6.6 shows the improvement on the iPAPR distribution for the CMPSK/4 when a rotation of π/M is performed every other symbol instant. It can be seen that at the 1% probability, the iPAPR can be reduced considerably for all the base constellations without affecting the detection performance. For the 4 options cases, only the CMPSK/4 modulations with rotation are going to be used in the continuation and will be noted as CMPSK/4 (without the "rot" suffix).

Finally, Figure 6.7a shows the iPAPR distribution of the CPSK modulations, all of them with roll-off = 0. When the order of the modulation increases, the PAPR decreases, and also, for the same order modulations, having just 3 options presents smaller PAPR than with 4 options, with the cost of reduced spectral efficiency (SE) (from 2 bits/symbol to 1.5 bits/symbol).

For further reduction of the iPAPR for the CMPSK/4 modulations, RRC filtering can be applied, and by doing this, the iPAPR is comparable with the ones presented by the CMPSK/3 modulations. In this comparisons (shown in Figure 6.7b) the CMPSK/4 modulations are filtered by an RRC filter with 0.25 roll-off factor, providing an spectral efficiency of 1.6 bps/Hz, against the 1.5 bps/Hz achieved with the CMPSK/3 modulations. However, as it will be seen in the next sections, the detection performance of the 3 options cases is better since 2 consecutive symbols can be used to correctly detect 3 bits, whereas for the 4 options case, just 1 received symbol is used to decode 2 bits.

After seeing that the PAPR of the signal can be decreased by increasing the number
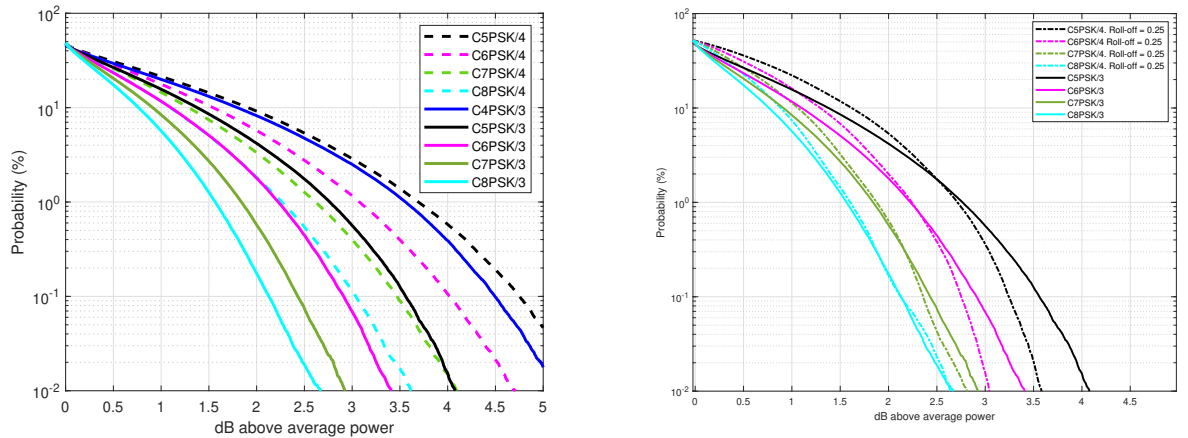
(a) *Comparison of the iPAPR of the CPSK modulations (3 and 4 options)*

(b) *Comparison of the iPAPR of the CPSK/4 modulations with RRC filtering and CPSK/3 modulations*

Figure 6.7. *CCDF distributions of PAPR for CPSK modulations with 3 and 4 options.*
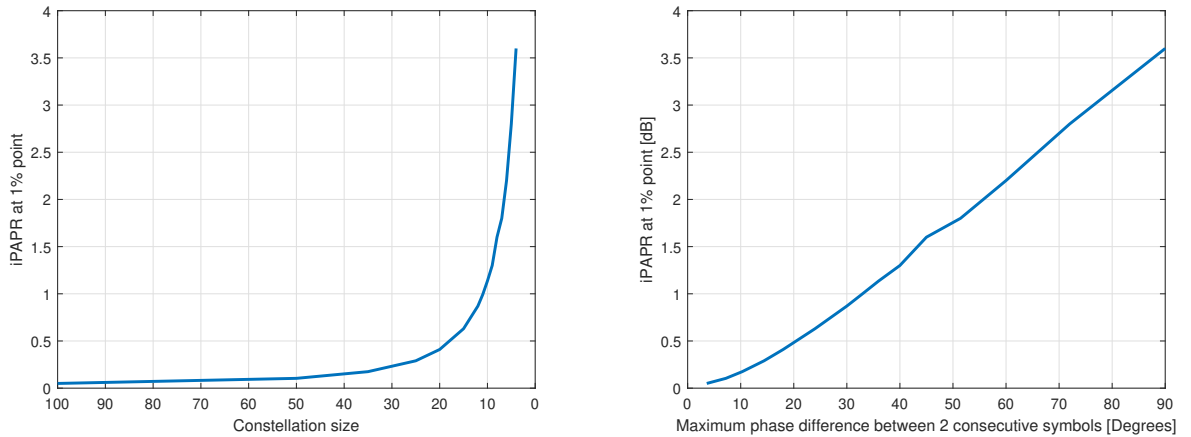
(a) *iPAPR increase with the number of options for CMPSK/3 modulations as a function of the constellation size*

(b) *iPAPR increase as a function of the maximum phase difference between 2 consecutive symbols for CMPSK/3 modulations*

Figure 6.8. *Effects of the number of the base PSK constellation on the sample-wise PAPR of the signal*

of constellation points of the base constellation, we can take a look at the evolution of the iPAPR values at 1% probability point with respect to the maximum phase difference between 2 consecutive symbols (this would be $2\pi/M$ radians or $2\pi/M \cdot \frac{180}{\pi}$ degrees, being M the number of symbols in the base constellation). Figure 6.8 shows that the increase in PAPR is linear with the maximum phase difference between 2 consecutive symbols. Obviously, when the constellation size increases (which is the same as the phase difference decreases), the envelope of the waveform becomes closer to constant but the constellations with higher number of symbols are not suitable for communications. This results however, allow us to think that these waveforms could be used to test different PA models, by generating a signal with a given PAPR.

Finally, Table 6.2 shows a summary of the iPAPR at 1% probability point for the different

Table 6.2. *iPAPR values at 1% probability point for the different modulations and roll-off factors*

Modulation	Roll-off = 0		Roll-off = 0.25		Roll-off = 0.5	
	iPAPR (dB)	SE (bps/Hz)	iPAPR (dB)	SE (bps/Hz)	iPAPR (dB)	SE (bps/Hz)
[1-D]$\pi/2$**-BPSK**	1.6	1.0	1.8	0.8	1.5	0.66
QPSK	4.5	2.0	3.5	1.6	2.5	1.3
$\pi/4$**-QPSK**	4.5	2.0	3.3	1.6	2.4	1.3
[1-D]$\pi/2$**-4PAM**	3.3	2.0	3.3	1.6	3.3	1.3
C4PSK/3	3.6	1.5	-	-	-	-
C5PSK/3	2.8	1.5	-	-	-	-
C6PSK/3	2.2	1.5	-	-	-	-
C7PSK/3	1.8	1.5	-	-	-	-
C8PSK/3	1.6	1.5	-	-	-	-
C5PSK/4	3.7	2.0	2.7	1.6	-	-
C6PSK/4	3.1	2.0	2.3	1.6	-	-
C7PSK/4	2.6	2.0	1.9	1.6	-	-
C8PSK/4	2.3	2.0	1.6	1.6	-	-

modulations that are going to be studied. For a SE of 1 bps/Hz, it is clear that the [1-D]$\pi/2$-BPSK presents a very low PAPR value. If the SE increases to 1.5 or 1.6 bps/Hz, the CPSK modulations with 3 options present a range of PAPR that goes from 3.4 dB down to 1.6 dB (increasing the order of the modulation helps to reduce the PAPR, but degrades the detection performance), and the RRC filtered C*M*PSK/4 modulations have similar PAPR than C*M*PSK/3, as mentioned before. QPSK and $\pi/4$-QPSK have a reduced PAPR when the RRC filter with roll-off 0.25, however, the filtered C*M*PSK/4 present the same SE and smaller PAPR. For 2 bps/Hz, the C*M*PSK/4 modulations have the smaller PAPR values (from 3.7 dB down to 2.3 dB, increasing the order of the modulation), and also [1-D]$\pi/2$-4PAM have more than 1 dB smaller PAPR, when compared to QPSK.

6.2 Maximum PA output power fulfiling OOB emission requirements

In this section, all the selected modulations are tested with the PA model defined in section 3.5.1. After the PA, the power spectral density (PSD) of the signal is calculated and compared to the IEEE mask (see Figure 6.9), which is the defined mask for IEEE 802.11ad. For these simulations, the SCS is 960 kHz, using 180 PRBs, which gives a channel bandwidth of 2.16 GHz, are used.

To compute the maximum output power per modulation (or find the minimum IBO), the following requirements need to be fulfilled (note that steps 2, 3 and 4 are 3GPP requirements):

1. The PSD of the transmitted signal fulfils the IEEE emission mask.
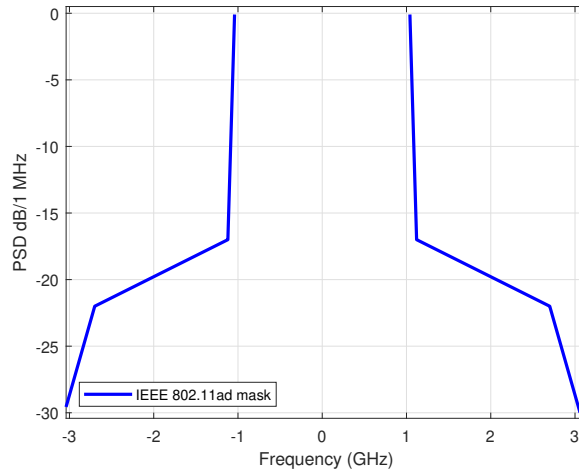
Figure 6.9. *IEEE mask for 2.16 GHz channel bandwidth*

2. 99 % of the signal power is inside the channel bandwidth.

3. The ACLR requirements are fulfilled (for the UL and DL).

4. The EVM requirements are fulfilled (for the UL and DL). At this point, we obtain the maximum output power from the IEEEad PA model.

At large, the UL and DL maximum output powers are different because the ACLR requirements change for both scenarios.

6.2.1 Maximum output power in the UL

In the UL, the minimum ACLR is 17 dB (see Section 3.3.1). As an example to see how the maximum output power is calculated following steps listed before, we can take a look at the QPSK modulation. After performing all the steps listed in the previous section, the obtained IBO for the QPSK was -8.3 dB. Figure 6.10 shows the PSD of the QPSK after the PA against the IEEE mask. For the QPSK, the limiting factor is the emission mask. This means, that if the IBO is reduced any further, the power spectral density (PSD) response of the signal after the PA will violate the emission mask. In this case. the obtained ACLR is 23.4 dB and the EVM is 9.0 %, and de maximum PA outpur power is 21.09 dBm.

Following the same steps, the maximum output power has been calculated for all modulations. Table 6.3 summarises the results. See appendix B to see a detailed table of all the parameters (ACLR, EVM) and limiting factor obtained with the maximum PA output power for all modulations. Also, in Table 6.3, the gap between the maximum PA output power for all the modulations against QPSK is noted. From that table, as it could be expected, the modulations with lower PAPR can achieve higher PA output power.
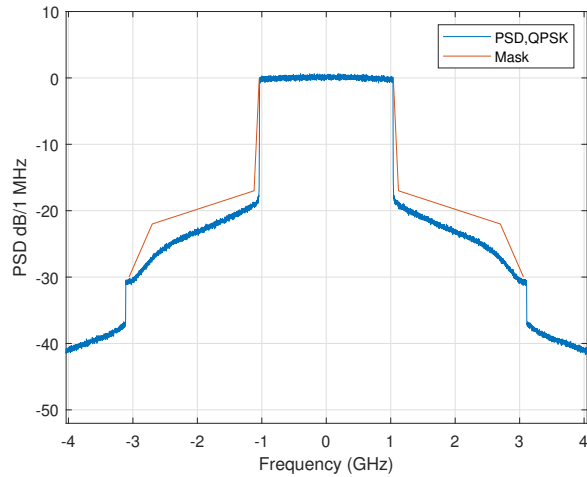
Figure 6.10. *PSD of the QPSK modulation after the PA. The IEEE modified mask is included for reference*

Table 6.3. *Maximum output power per modulation fulfilling all requirements for the UL*

Modulation	Pout [dBm]	Gap against QPSK [dB]
QPSK	21.09	0
[1-D]$\pi/2$-4PAM	23.56	2.47
C5PSK/4	22.79	1.70
C6PSK/4	24.17	3.08
C7PSK/4	25.00	3.91
C8PSK/4	25.26	4.17
$\pi/4$-QPSK$_{\alpha=0.25}$	22.15	1.06
C5PSK/4$_{\alpha=0.25}$	24.07	2.98
C6PSK/4$_{\alpha=0.25}$	25.26	4.17
C7PSK/4$_{\alpha=0.25}$	25.26	4.17
C8PSK/4$_{\alpha=0.25}$	25.26	4.17
C4PSK/3	23.28	2.19
C5PSK/3	24.73	3.64
C6PSK/3	25.26	4.17
C7PSK/3	25.26	4.17
C8PSK/3	25.26	4.17
[1-D]$\pi/2$-BPSK	25.26	4.17

6.2.2 Maximum output power in the DL

In the DL, the minimum ACLR is 28 dB (see Section 3.3.1). Performing the same steps as for the UL, the maximum output power per modulation can be seen in Table 6.4. (Note that the PA saturation power with the model used is 25.26 dBm). For the DL, the gaps with respect to QPSK are bigger than in the UL case, this is due to the fact that the maximum PA output power of QPSK is ACLR limited (also, in Appendix B, a more detailed Table is shown for the DL).

Table 6.4. Maximum output power per modulation fulfilling all requirements for the DL

Modulation	Pout [dBm]	Gap against QPSK [dB]
QPSK	18	0
[1-D]$\pi/2$-4PAM	21.14	3.14
C5PSK/4	19.72	1.72
C6PSK/4	21.27	3.27
C7PSK/4	22.65	4.65
C8PSK/4	23.75	5.75
$\pi/4$-QPSK$_{\alpha=0.25}$	20.20	2.20
C5PSK/4$_{\alpha=0.25}$	22.35	4.35
C6PSK/4$_{\alpha=0.25}$	24.21	6.21
C7PSK/4$_{\alpha=0.25}$	25.26	7.26
C8PSK/4$_{\alpha=0.25}$	25.26	7.26
C4PSK/3	20.17	2.17
C5PSK/3	22.11	4.11
C6PSK/3	23.73	5.73
C7PSK/3	25.09	7.09
C8PSK/3	25.26	7.26
[1-D]$\pi/2$-BPSK	25.26	7.26

6.3 Theoretical SER for underlying PSK constellations

Since the base constellations used for the CPSK modulations have the same or more symbols than in the QPSK modulation, it is expected to have some degradation on the detection performance due to the smaller Euclidean distance between the symbols when the number of symbols increases. As defined in [18, Sec. 4.3-2], the symbol error probability (P_s) for PSK modulations with large values of M and SNR, under AWGN channel can be approximated by

$$P_s \approx 2Q\left(\sqrt{2\gamma_s}sin(\frac{\pi}{M})\right) \tag{6.1}$$

where γ_s is the SNR per symbol ($E_s/N0$) and M is the constellation order. Thus the achievable SER for base PSK constellation from 4 to 8 symbols is shown in Figure 6.11, showing the expected degradation in the detection when the number of symbol increases. Assuming that all the constellations carry the same amount of bits per symbols, the SNR differences in SER are directly mapped into SNR differences in BER, and therefore, the SNR gap presented on this comparison would have to be compensated by the maximum PA output power achievable for each modulation in order to compete with QPSK, or use the inherent memory of the CPSK modulations at the receiver side in order to close the gap. The theoretical SNR gaps are shown in Table 6.5.

Seeing the results from Table 6.5, the SNR gap between the 7PSK and 8PSK against
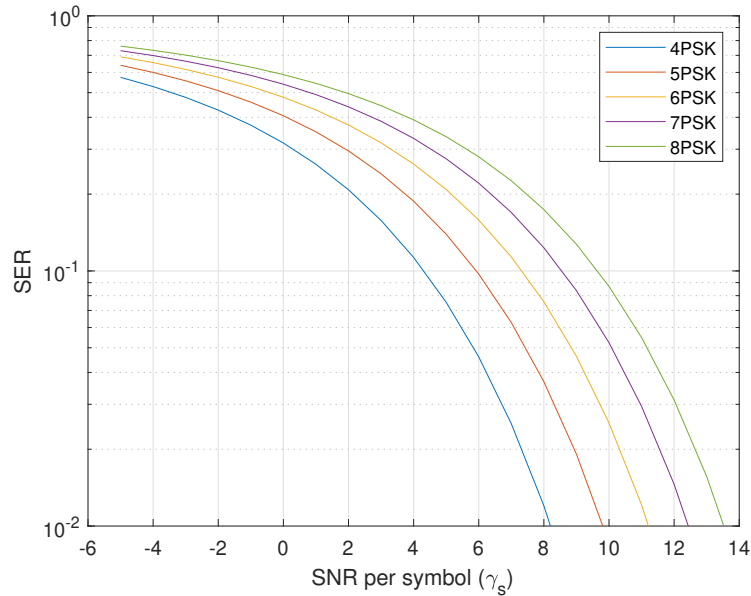
Figure 6.11. SER for different PSK constellations

Table 6.5. SNR per symbol needed to achieve 10% SER for different PSK constellations

Base PSK modulation	γ_s at 10% SER	Gap to QPSK
4PSK	4.3 dB	0 dB
5PSK	5.9 dB	-1.6 dB
6PSK	7.3 dB	-3.0 dB
7PSK	8.5 dB	-4.2 dB
8PSK	9.6 dB	-5.3 dB

4PSK (or QPSK) is bigger or close to the maximum difference of PA maximum output power of C7PSK and C8PSK on the UL (see table 6.3), therefore, making C7PSK and C8PSK difficult to be useful for communications. C7PSK and C8PSK with 3 and 4 options are not going to be included in the comparisons due to the expected performance loss in the detection.

6.4 Link performance evaluations over AWGN channel

After the PAPR and maximum PA output power studies, all the modulations that are worth to compare, have to be tested under link performance evaluations over AWGN channel in order to note the needed Signal to Noise Ratio (SNR) per modulation to have 7 % and 30 % BER with uncoded transmissions. These numbers are chosen accordingly to the SRN ranges where the channel coding schemes work with QPSK modulation as defined in the MCS tables on Release 15 [30].

We can get the BER performance over AWGN channel for all the selected modulations (see Figure 6.12). Note here that the RRC filtered modulations ($\pi/4$-QPSK and
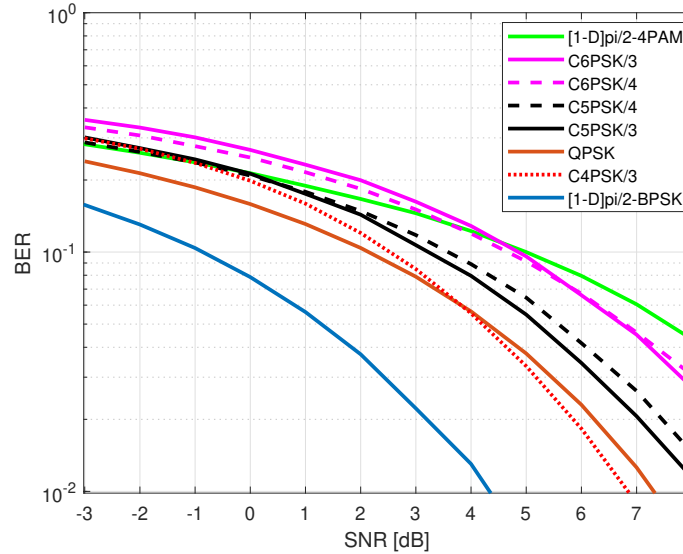
Figure 6.12. *BER vs SNR for the selected modulations*

C*M*PSK/4) have the same BER performance as when the RRC filter is not applied for the same modulation, that is why they have not been included in the illustrations. For the CPSK modulations, a BCJR algorithm [29] has been used in the receiver in order to exploit the inherent memory from the CPSK modulations at the receiver side.

Table 6.6 summarises the SNR needed for each modulation to reach 7 % and 30 % BER. For the [1-D]$\pi/2$-4PAM modulation, there is a gap of 3 dB with respect to QPSK in the SNR needed to reach 7 % BER, therefore making it not suitable for communications due to the performance loss in the detection. For the C*M*PSK/3 modulations, these results show that the gap in BER with respect to QPSK is smaller than the theoretical one calculated in Section 6.3, this is because the information of 2 consecutives symbols can be use to detect the bits. The effect of increasing the base constellation size for CPSK modulations can also be seen from the results. The C*M*PSK/3 modulations present smaller gap against QPSK when the BER decreases than the RRC filtered C*M*PSK/4.

6.5 Link performance evaluations over AWGN channel with PN

The effects of the PN are introduced in order to see the robustness of the modulations against PN. The SCS used for these simulations is 120 kHz and the carrier frequency is 60 GHz. Ideal CPE compensation is applied in the receiver side.

Figure 6.13 shows the BER performance against the SNR when the PN is included and Table 6.7 summarises the needed SNR to achieve 7% and 30 % BER for the selected modulations. As expected, all the modulations present a worse BER performance since the PN degrades the detection. The gap between the CPSK modulations and QPSK increases slightly compared to the case where the PN is not present (important to note

Table 6.6. *SNR needed for 7 % and 30 % BER for the selected modulations (AWGN channel)*

Modulation	SNR @30% BER [dB]	SNR @7% BER [dB]	Gap @30% BER with QPSK [dB]	Gap @7% BER with QPSK [dB]
QPSK	-5.6	3.4	0.0	0.0
[1-D]π/2-4PAM	-3.8	6.4	-1.8	-3
C5PSK/4	-3.4	4.7	-2.2	-1.3
C6PSK/4	-1.9	5.9	-3.7	-2.5
$\pi/4$-QPSK$_{\alpha=0.25}$	-5.6	3.4	0.0	0.0
C5PSK/4$_{\alpha=0.25}$	-3.4	4.7	-2.2	-1.3
C6PSK/4$_{\alpha=0.25}$	-1.9	5.9	-3.7	-2.5
C4PSK/3	-3.0	3.5	-2.6	-0.1
C5PSK/3	-3.0	4.3	-2.6	-0.9
C6PSK/3	-1.0	5.9	-4.6	-2.5
[1-D]π/2-BPSK	-8.7	0.3	3.0	3.0
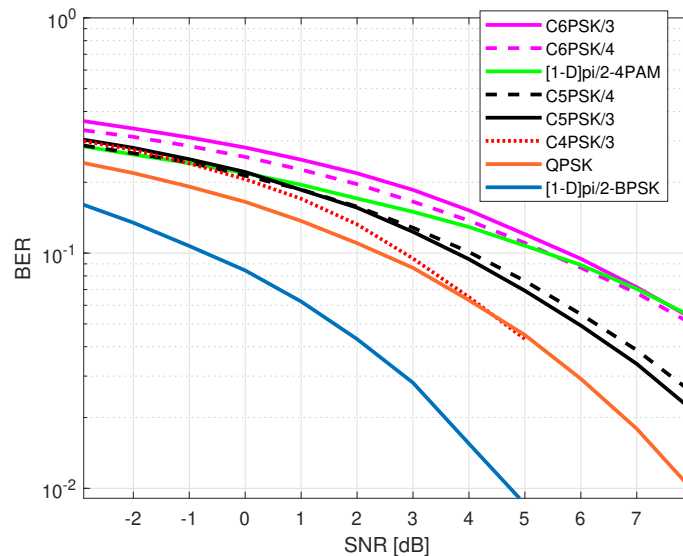
Figure 6.13. *BER vs SNR for the selected modulations with PN. SCS = 120 kHz, fc = 60 GHz*

here that the performance gap between C4PSK/3 and QPSK remains the same with and without PN). This can be also explained with the smaller Euclidean distances when the base constellation size increases. It has to be noted here that the performance of the CPSK modulations depends heavily on the detection algorithm used at the receiver side.

Table 6.7. *SNR needed for 7 % and 30 % BER for the selected modulations including the effects of PN. SCS = 120 kHz, fc = 60 GHz*

Modulation	SNR @30% BER [dB]	SNR @7% BER [dB]	Gap @30% BER with QPSK [dB]	Gap @7% BER with QPSK [dB]
QPSK	-5.5	3.7	0	0
[1-D]π/2-4PAM	-3.9	7.0	-1.6	-3.3
C5PSK/4	-3.4	5.2	-2.1	-1.5
C6PSK/4	-1.6	6.7	-3.9	-3.0
$\pi/4$-QPSK$_{\alpha=0.25}$	-5.5	3.7	-0.0	0.0
C5PSK/4$_{\alpha=0.25}$	-3.4	5.2	-2.1	-1.5
C6PSK/4$_{\alpha=0.25}$	-1.6	6.7	-3.9	-3.0
C4PSK/3	-2.9	3.8	-2.6	-0.1
C5PSK/3	-2.8	4.9	-2.7	-1.2
C6PSK/3	-0.7	7.1	-4.8	-3.4
[1-D]π/2-BPSK	-8.5	0.6	3.0	3.1

6.6 Link budget gain per modulation

With all the results obtained in the previous sections, the final step to see which one of the candidates performs better, is to compare them accordingly to their SNR needed to achieve a given BER value and also the maximum PA output power available, defined as the link budget gain (LBG).

In this project, the reference modulation is the QPSK, and the LBG is defined as

$$LBG_{@x\%BER} = (P_{outmod} - P_{outQPSK}) + (SNR_{QPSK@x\%BER} - SNR_{mod@x\%BER}) \quad (6.2)$$

where P_{outmod} is the maximum PA output power for the modulation being compared, $P_{outQPSK}$ is the maximum output power for the QPSK and $SNR_{mod@x\%BER}$ and $SNR_{QPSK@x\%BER}$ are the SNR needed for the modulation being compared and for QPSK to achieve $x\%$ BER, respectively. All values are given in dB.

6.6.1 Link budget gain in the UL

In the UL, the LBG obtained for each modulation against QPSK under AWGN channel and AWGN with PN channel is shown in Table 6.8. It can be seen that the C5PSK/4 and C6PSK/4, carrying the same amount of bits as the QPSK, present a positive LBG. Worth to mention here that the C5PSK/4 and C6PSK/4 with RRC filtering have greater LBG than $\pi/4$-QPSK with RRC filtering. As a trend, it is seen that for the CPSK modulations, when

Table 6.8. *Link Budget Gain at 7 % and 30 % BER for the selected modulations in AWGN and AWGN + PN channels for the UL with the IEEE mask as reference.*

Modulation	LBG @30% BER [dB] (AWGN)	LBG @30% BER [dB] (AWGN+PN)	LBG @7% BER [dB] (AWGN)	LBG @7% BER [dB] (AWGN+PN)
QPSK	0	0	0	0
[1-D]$\pi/2$-4PAM	0.7	0.9	-0.5	-0.8
C5PSK/4	-0.5	-0.4	0.4	0.2
C6PSK/4	-0.6	-0.8	0.6	0.1
$\pi/4$-QPSK$_{\alpha=0.25}$	1.1	1.1	1.1	1.1
C5PSK/4$_{\alpha=0.25}$	0.8	0.9	1.7	1.5
C6PSK/4$_{\alpha=0.25}$	0.5	0.3	1.7	1.2
C4PSK/3	-0.4	-0.4	2.1	2.1
C5PSK/3	1.0	0.9	2.8	2.4
C6PSK/3	-0.4	0.6	1.7	0.8
[1-D]$\pi/2$-BPSK	7.2	7.2	7.2	7.3

the uncoded BER decreases, the LBG increases. The gain of the $\pi/4$-QPSK is directly the difference in maximum PA output power. As expected, the [1-D]$\pi/2$-BPSK, present the maximum LBG, although its SE is the lowest of all the modulations. And finally, the [1-D]$\pi/2$-4PAM, just shows positive LBG for high BER with respect to QPSK. Comparing the values when the PN is added, the CPSK modulations lose some LBG, but overall maintain the gain.

Interesting to note here the gain of the CMPSK/3 (with M=4, 5 and 6), where the C5PSK/3 can provide 2.8 dB of LBG at 7% uncoded BER. At the same BER, the C5PSK/3 provides also bigger LBG than the $\pi/4$-QPSK with RRC filtering.

6.6.2 Link budget gain in the DL

For the DL scenario, the same comparisons are done. Table 6.9 shows the LBG for the modulations.

In this case, it has to be noted that for both AWGN and AWGN with PN channels, all the CPSK modulations present positive LBG at lower BER, also important to note here that the LGB that the C6PSK/4 with RRC filtering shows at 7% BER 3.7 dB of LBG (C4PSK/3, C5PSK/3 and C6PSK/3 also present LBG bigger than 2 dB). Including RRC filtering, the LBG with CPSK modulations are equal or bigger than RRC filtered $\pi/4$-QPSK. One important result that comes from these evaluations is that [1-D]$\pi/2$-BPSK is showing a LBG greater than 10 dB for the DL, therefore, making it a good candidate to be included for the DL (currently it is only accepted for the UL).

Table 6.9. *Link Budget Gain at 7 % and 30 % BER for the selected modulations in AWGN and AWGN + PN channels for the DL with the IEEE mask as reference.*

Modulation	LBG @30% BER [dB] (AWGN)	LBG @30% BER [dB] (AWGN+PN)	LBG @7 % BER [dB] (AWGN)	LBG @7% BER [dB] (AWGN+PN)
QPSK	0	0	0	0
[1-D]π/2-4PAM	1.3	1.5	0.1	-0.1
C5PSK/4	-0.5	-0.4	0.4	0.2
C6PSK/4	-0.4	-0.6	0.8	0.3
$\pi/4$-QPSK$_{\alpha=0.25}$	2.2	2.2	2.2	2.2
C5PSK/4$_{\alpha=0.25}$	2.2	2.3	3.1	2.9
C6PSK/4$_{\alpha=0.25}$	2.5	2.3	3.7	3.2
C4PSK/3	-0.4	-0.4	2.1	2.1
C5PSK/3	1.5	1.4	3.2	2.9
C6PSK/3	1.1	1.0	3.2	2.3
[1-D]π/2-BPSK	10.3	10.3	10.3	10.4

6.7 Coded performance

As a final comparison, the performance of some of the modulations are tested by using a 5G NR compliant link simulator. For these comparisons, the QPSK, [1-D]π/2-BPSK, C*M*PSK/4 (with M = 5 and 6) and C*M*PSK/3 (with M = 4, 5 and 6) are encoded with a low-density parity-check (LDPC) code following 5G NR specifications [25], with different coding rates, such as R = 1/3, 2/3 and 4/5, which correspond to a physical BER of 20%, 10% and 4%, approximately, to get 10% Block Error Rate (BLER), defined as the ratio of incorrectly decoded blocks out of the total number of transmitted coded blocks. This simulations are done to validate the previously obtained LBG results with uncoded BER.

Simulations with AWGN channel have been performed for the modulations listed before, as well as AWGN with PN channel. Also, TDL-E channel as defined in [31], with 3 km/h of user mobility, has been used for the simulations to test the performance of the CPSK modulations with multipath channels (in the receiver, ideal channel estimation has been used). The LBG for coded performance is calculated at 10% BLER as

$$LBG_{@10\%BLER} = (P_{outmod} - P_{outQPSK}) + (SNR_{QPSK@10\%BLER} - SNR_{mod@10\%BLER})$$

$$(6.3)$$

where the maximum PA output power are the ones computed in section 6.2.
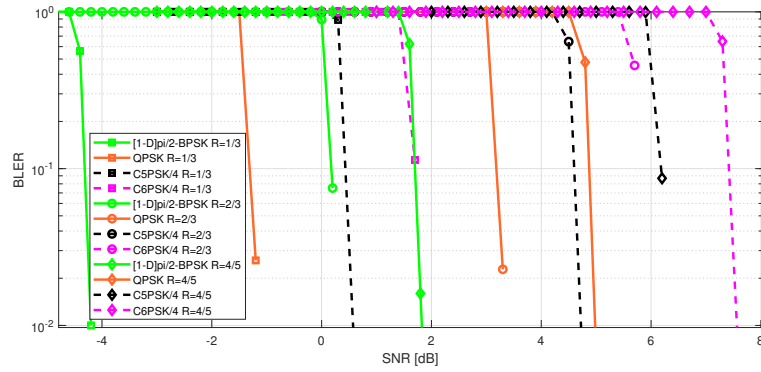
(a) BLER of [1-D]π/2-BPSK, QPSK and CMPSK/4 (M = 5 and 6)
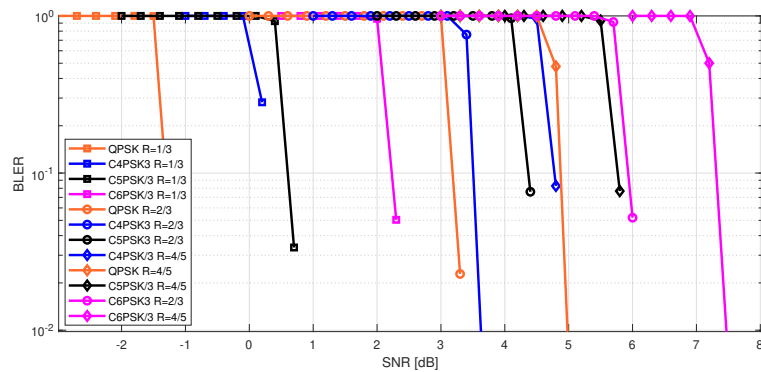
(b) BLER of QPSK and CMPSK/3 (M = 4, 5 and 6)

Figure 6.14. *Coded link performance of the selected modulations and coding rates (AWGN channel).*

6.7.1 Coded Link performance evaluation

In this section, the final coded results of the link performance simulations run with the 5G NR compliant link simulator are shown. The Figures 6.14 to 6.16 illustrate the BLER results for the different modulations and coding rates selected for comparisons. Those results show that the coded performance can be directly mapped to the uncoded BER performance from the previous section. When looking at the TDL-E with PN results, we can see that C4PSK/3 with R=4/5 achieves the 10% BLER with 6.8 dB of SNR, while QPSK with the same rate, needs 7 dB of SNR. And as expected, [1-D]π/2-BPSK requires less SNR to achieve the same BLER than the rest modulations.

It has to be noted here, that the link performance of the CPSK modulations depends on the receiver implementation.

6.7.2 Coded Link Budget Gain in the UL

The same way as it was done in section 6.6, the coded LBG is divided into UL LBG and DL LBG. Table 6.10 shows the LBG of the modulations for the UL with AWGN channel. It can be seen that for a rate R = 2/3, the coded LBG matches with the uncoded LBG calculated in the previous section. Also, as noted before, when the coding rate increases,
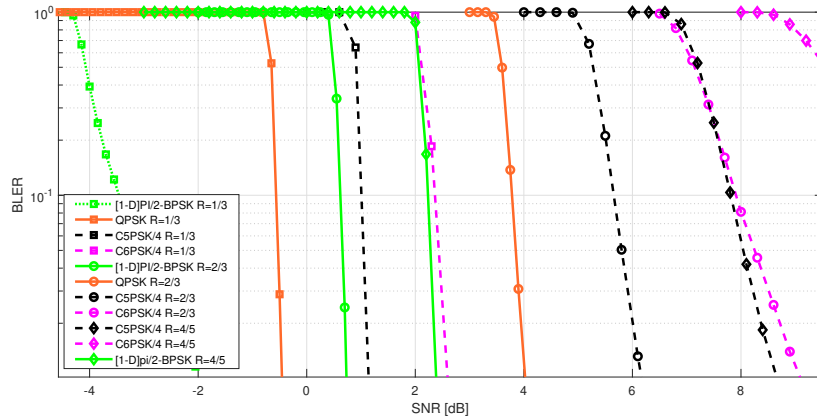
(a) BLER of [1-D]π/2-BPSK, QPSK and CMPSK/4 (M = 5 and 6)
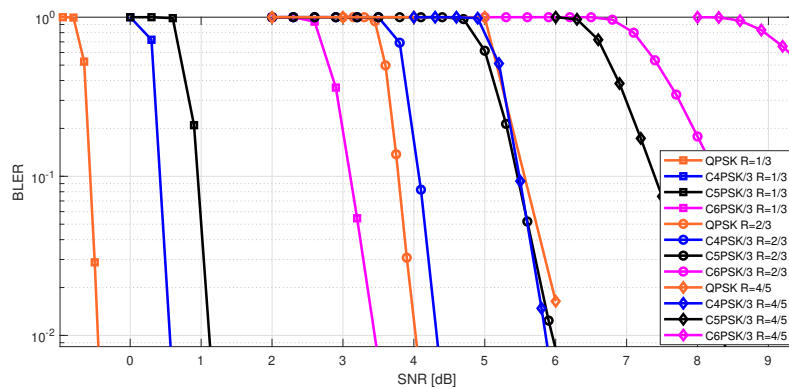
(b) BLER of QPSK and CMPSK/3 (M = 4, 5 and 6)

Figure 6.15. *Coded link performance of the selected modulations and coding rates (AWGN and PN channel).*

the LBG also increases. From these results, we can say that in scenarios were PN is not dominant, the CPSK modulations can provide up to 2.5 dB of LBG (C5PSK/3 with R=4/5) and that the CMPSK/4 modulations, with the same SE than QPSK, are showing positive LBG. Therefore, if the PN is not dominant, we can conclude that CPSK modulations allows to use the PA in a more efficient way without losing SE (in the 4 options cases), or provide around 2 dB of LBG (for the 3 options cases) losing some SE. The LBG that $\pi/4$-QPSK was showing from the previous sections was directly the difference in maximum power, and it was 1.1 dB, therefore, the CMPSK/3 modulations when using coding rates greater than 1/3 are already performing better than $\pi/4$-QPSK, also as special case, C5PSK/3 with R=1/3 is presenting 1.7 dB of LBG, i.e., 0.6 dB better than $\pi/4$-QPSK with RRC filtering.

Table 6.11 shows the coded LBG for the UL when the effects of PN are added in the simulations. These result show that at lower coding rate, the CPSK modulations with 3 options present larger LBG than without PN (C4PSK/3 shows 0.5 dB larger LBG and C5PSK/3 shows 0.4 dB larger LBG with R=1/3). When the PN is included, CPSK modulations with 4 options do not present LBG when the coding rate increases, with the current receivers. These results are still in line with the uncoded results shown in Table 6.8.
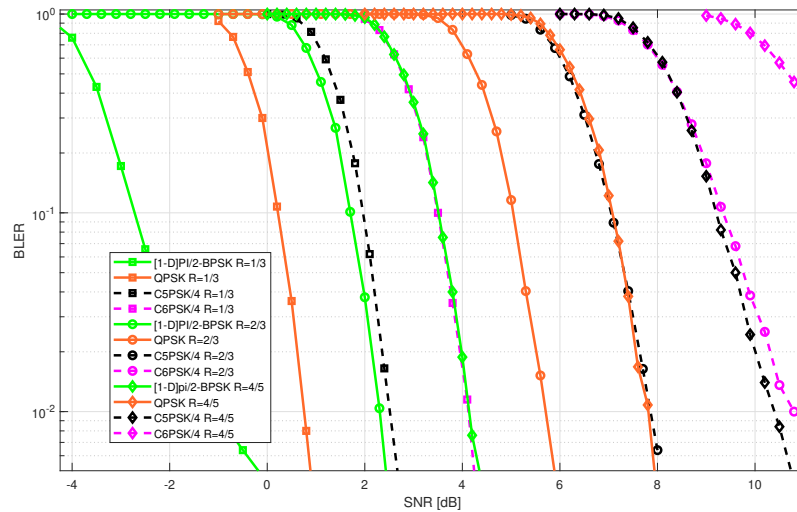
(a) BLER of [1-D]π/2-BPSK, QPSK and CMPSK/4 (M = 5 and 6)
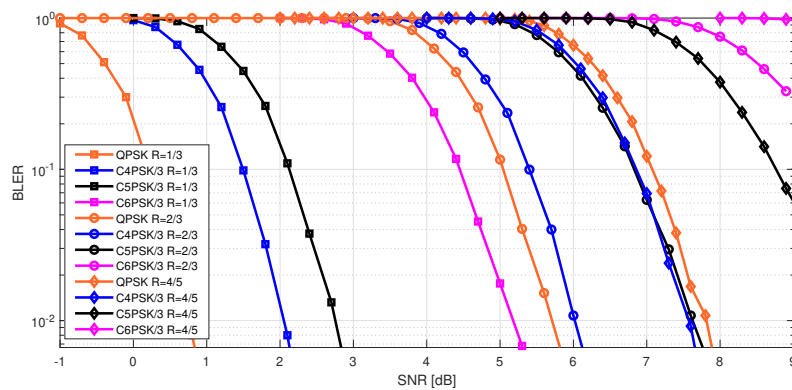
(b) BLER of QPSK and CMPSK/3 (M = 4, 5 and 6)

Figure 6.16. *Coded link performance of the selected modulations and coding rates (TDL-E and PN channel).*

Finally, Table 6.15 shows the UL LBG when a TDL-E channel with PN is used in the simulations. This is a miltipath channel, and the results reveal that C4PSK/3 with higher coding rate presents 2.5 dB of LBG and C5PSK/3 presents between 1.7 and 1.9 dB of LBG for all the tested coding rates. For both (C4PSK/3 and C5PSK/3), the LBG at higher coding rates are greater than with the AWGN channel with PN, meaning that these modulations do not suffer severe degradation when multipath channels are included. Even with TDL-E channel and PN, CMPSK/3 modulations show larger LBG than $\pi/4$-QPSK with RRC filtering, which in section 6.6 was found to be 1.1 dB for the UL.

6.7.3 Coded Link Budget Gain in the DL

For the DL, Table 6.13 shows the LBG per modulation with AWGN channel. Comparing with Table 6.10 (it shows the same LBG, but for the UL), we can observe than overall, the LBG that the modulations show under AWGN channel is very similar for both cases,

Table 6.10. UL Link Budget Gain against QPSK for the selected code rates in AWGN channel.

Modulation	LBG (R = 1/3) [dB]	LBG (R=2/3) [dB]	LBG (R = 4/5) [dB]
[1-D]$\pi/2$-BPSK	+7.2	+7.2	+7.4
C4PSK/3	+0.7	+1.9	+2.3
C5PSK/3	+1.7	+2.4	+2.5
C6PSK/3	+0.7	+1.4	+1.8
C5PSK/4	0.0	+0.3	+0.4
C6PSK/4	+0.1	+0.6	+0.6

Table 6.11. UL Link Budget Gain against QPSK for the selected code rates in AWGN with PN channel.

Modulation	LBG (R = 1/3) [dB]	LBG (R=2/3) [dB]	LBG (R = 4/5) [dB]
[1-D]$\pi/2$-BPSK	+8.3	+7.4	+7.5
C4PSK/3	+1.2	+1.9	+2.2
C5PSK/3	+2.1	+1.9	+1.7
C6PSK/3	+0.5	-0.3	-1.3
C5PSK/4	+0.1	-0.2	-0.6
C6PSK/4	+0.1	-0.9	-3.7

Table 6.12. UL Link Budget Gain against QPSK for the selected code rates in TDL-E with PN channel.

Modulation	LBG (R = 1/3) [dB]	LBG (R=2/3) [dB]	LBG (R = 4/5) [dB]
[1-D]$\pi/2$-BPSK	+7.1	+7.5	+7.7
C4PSK/3	+0.9	+1.8	+2.5
C5PSK/3	+1.7	+1.8	+1.9
C6PSK/3	-0.1	-0.6	-1.1
C5PSK/4	-0.1	-0.3	-0.5
C6PSK/4	-0.2	-1.2	-2.2

Table 6.13. *DL Link Budget Gain against QPSK for the selected code rates in AWGN channel.*

Modulation	LBG (R = 1/3) [dB]	LBG (R=2/3) [dB]	LBG (R = 4/5) [dB]
[1-D]$\pi/2$-BPSK	+10.3	+10.3	+10.4
C4PSK/3	+0.7	+1.9	+2.3
C5PSK/3	+2.2	+2.9	+2.5
C6PSK/3	+2.2	+2.9	+1.8
C5PSK/4	+0.0	+0.3	+0.4
C6PSK/4	+0.3	+0.8	+0.6

Table 6.14. *DL Link Budget Gain against QPSK for the selected code rates in AWGN with PN channel.*

Modulation	LBG (R = 1/3) [dB]	LBG (R=2/3) [dB]	LBG (R = 4/5) [dB]
[1-D]$\pi/2$-BPSK	+11.3	+10.4	+10.5
C4PSK/3	+1.2	+1.9	+2.2
C5PSK/3	+2.6	+2.4	+2.2
C6PSK/3	+2.0	+1.2	+0.2
C5PSK/4	+0.1	-0.2	-0.6
C6PSK/4	+0.3	-0.8	-3.5

the main difference is that for the DL, the LBG with lower coding rates for C5PSK/3 and C6PSK/3 is greater. With the current receiver, in AWGN channels for the DL, around 2 dB of LBG can be obtained for C*M*PSK/3 modulations, while C*M*PSK/4 also show positive LBG.

Table 6.14 shows the LBG in the DL when the PN is added. In this case, C5PSK/3 is the modulation showing the greatest LBG for all the simulated coding rates. Looking at these results, we can conclude that C*M*PSK/3 modulations are shown to be robust against PN, due to the fact that the LBG is maintained when the PN is included.

Finally, Table 6.15 shows the LBG in the DL with the TDL-E channel with PN. It can be seen that the LBG of the C*M*PSK/3 modulations is positive, and that C5PSK/3 can provide more than 2 dB of LBG against QPSK for all the simulated coding rates, even with multipath channels.

Moreover, it is worth to mention here that [1-D]π/2-BPSK shows more than 10 dB of LBG in the DL for all the channels and coding rates evaluated. These are good results to promote [1-D]π/2-BPSK also in the DL, since the receiver complexity does not increase and the PA could be used very efficiently.

Table 6.15. DL Link Budget Gain against QPSK for the selected code rates in TDL-E with PN channel.

Modulation	LBG (R = 1/3) [dB]	LBG (R=2/3) [dB]	LBG (R = 4/5) [dB]
[1-D]$\pi/2$-BPSK	+10.1	+10.6	+10.7
C4PSK/3	+0.9	+1.8	+2.5
C5PSK/3	+2.2	+2.3	+2.3
C6PSK/3	+1.4	+0.9	+0.4
C5PSK/4	-0.1	-0.3	-0.5
C6PSK/4	+0.0	-1.0	-2.0

7 CONCLUSIONS AND FUTURE WORK

7.1 Conclusions

In this thesis, different modulations for DFTs-OFDM have been tested in order to compare their performance with non-idealities that are present in communications above 52.6 GHz, such as PA non-linearities and severe PN. In addition to that, a new technique to map bits to symbols for PSK modulations is presented, applying a constraint in order to reduce the PAPR of the signals, denoted as constrained PSK (CPSK).

Comprehensive link level simulations were carried out to evaluate several modulation candidates. Based on these evaluations, the new proposed CPSK modulations are shown to reduce the PAPR of the signal considerably, a really important characteristic for mmWave communications. Also, when computing the LBG with the current receivers, these modulations present positive LBG, (specially CMPSK/3 modulations or CMPSK/4 with RRC filtering for the different channels tested). Therefore making them good candidates to be used as power-efficient modulations for mmWave or satellite communications.

Finally, due to the fact that CPSK modulations can be used with DFTs-OFDM, it would be easy to include them into future specifications without performing big changes in the current ones. The different parameters needed (e.g., order of the base constellation, number of options, mapping tables, etc) could be signalised by a control channel indicator, such as MCS index, currently used in LTE and 5G NR, pointing to a specific configuration table previously defined. Given the nature of the CPSK modulations, 5G NR reference signals (such as phase tracking reference signal (PTRS) for CPE estimation) can be included at the beginning of each CPSK block, without altering the waveform characteristics. In this work both the UL and DL LBG have been computed. However, these modulations are mostly thought to be used in the UL. The reason behind is because the UEs are more restricted in power than the base stations and, the receiver algorithms may present greater complexity than the traditional ones.

In Section 6.1.4, it is observed that the sample-wise PAPR decreases when the base constellation size increases. Therefore, another use for CPSK modulations with DFTs-OFDM is that they could be used to generate different waveforms with a selected sample-wise PAPR by increasing the constellation size of CMPSK/3, with M = 8, 9, 10, 11, etc. Moreover, they can be utilised to test different PA models, mapping the PA output power with the sample-wise PAPR that the waveforms present at a certain level.

In addition to the CPSK modulations, based on all the evaluations made on this work, the results have shown that pulse shaped $\pi/2$-BPSK presents the highest LBG of all the modulations tested. In particular for the DL, the LBG was found to be greater than 10 dB in all the evaluated scenarios. Therefore making it a suitable candidate to be included also in the DL, since the complexity of the transmitter and receiver does not increase compared to the traditional ones.

7.2 Future work

After this project, some future work can still be done. For example, in the transmitter side, filtering can be performed in order to further reduce the PAPR, but respecting the OOB and EVM limits set by the specifications without losing SE. By doing this, it could be possible to increase the LBG of the CPSK modulations.

Also, in the receiver side there is an important open field of research in order to further reduce the SNR gap between the CPSK modulations and QPSK, without affecting the PAPR of the signal. This can be done by an smart use of the inherent memory that the CPSK modulations present, or by the inclusion of receiver filters to exploit the low pass characteristic shape of the PSD of the CPSK signals, that would allow to reduce the noise at the receiver side.

Finally, following the same ideas, different new constrained modulations that are not based only on PSK modulations can be tested.

REFERENCES

[1]   E. Dahlman, S. Parkvall and J. Sköld. *5G NR: The Next Generation Wireless Access Technology*. 1st ed. Mara Conner. ISBN: 978-0-12-814323-0.

[2]   vivo. *Use case and design requirements for NR beyond 52.6 GHz*. Mar. 18, 2019.

[3]   3GPP. *3GPP TR 38.805 V14-0.0. 3rd Generation Partnership Project; Technical Specification Group Radio Access Network; Study on New Radio access technology; 60 GHz unlicensed spectrum (Release 14)*. 2017.

[4]   3GPP. *ETSI TR 138 913 V14.2.0 (2017-05); 5G; Study on Scenarios and Requirements for Next Generation Access Technologies (3GPP TR 38.913 version 14.2.0 Release 14)*. 2017.

[5]   3GPP. *ETSI TR 138 901 V14.1.1 (2017-08); 5G; Study on channel model for frequencies from 0.5 to 100 GHz (3GPP TR 38.901 version 14.1.1 Release 14)*. 2017.

[6]   Intel. *TR 38.807-004: Study on requirements for NR beyond 52.6 GHz*. 2018.

[7]   3GPP. *3GPP TR 38.807. 3rd Generation Partnership Project; Technical Specification Group Radio Access Network; Study on requirements for NR beyond 52.6 GHz (Release 16)*. June 2019.

[8]   R. W. H. Robert C. Daniels. 60 GHz wireless communications: Emerging requirements and design recommendations. *IEEE Vehicular Technology Magazine* 2.3 (Sept. 2007), 41–50.

[9]   3GPP. *3GPP TR 38.803 V14.2.0 (2017-09); 3rd Generation Partnership Project; Technical Specification Group Radio Access Network; Study on new radio access technology: Radio Frequency (RF) and co-existence aspects (Release 14)*. 2017.

[10]   3GPP. *3GPP TS 38.104. 3rd Generation Partnership Project; Technical Specification Group Radio Access Network; NR; Base Station (BS) radio transmission and reception (Release 15)*. Mar. 2019.

[11]   3GPP. *3GPP TS 38.101-2. 3rd Generation Partnership Project; Technical Specification Group Radio Access Network; NR; User Equipment (UE) radio transmission and reception; Part 2: Range 2 Standalone (Release 15)*. Dec. 2018.

[12]   K. Zeng, H. Cai, G. Wang and Y. Xin. *Considerations on Phase Noise Model for 802.11ay*. 2016.

[13]   A. G. Armada and M. Calvo. Phase Noise and Sub-Carrier Spacing Effects on the Performance of an OFDM Communication System. *IEEE Communications letter* Vol 2.Number 1 (), 1–4.

[14]   Zhijian Li, L. P. Ligthart, Peikang Huang, Weining Lu, W. F. van der Zwan, E. P. Lys and O. A. Krasnov. Phase Noise and Sub-Carrier Spacing Effects on the Performance of an OFDM Communication System. *MIKON 2008 - 17th International Conference on Microwaves, Radar and Wireless Communications* (), 11–13.

[15] Lianming LI, Dongming WANG1, Xiaokang NIU1, Yuan CHAI, Linhui CHEN, Long HE, Xu WU, Fuchun ZHENG, Tiejun CUI, Xiaohu YOU. mmWave communications for 5G: implementation challenges and advances. *SCIENCE CHINA Information Sciences* 61.2 (July 2017).

[16] *IEEE P802.11 Wireless LANs. PHY/MAC Complete Proposal Specification*. May 18, 2010.

[17] NASA. *DESCANSO - Chapter 2. Constant Envelope Modulations*.

[18] J. G. Proakis and M. Salehi. *Digital Communications*. 5th. McGraw-Hill, 2008. ISBN: 978-0-07-295716-7.

[19] H. G. M. David J. Goodman. *Single Carrier FDMA. A New Air Interface for long Term Evolution*. 1st ed. Vol. 1. ISBN: 978-0-470-72449-1 (HB).

[20] IEEE. *IEEE 802.11-17/1292r1. IEEE P802.11 Wireless LANs. Draft text to define non-uniform constellation*. Sept. 2017.

[21] ETSI. *ETSI EN 302 307-1 V1.4.1. Digital Video Broadcasting (DVB); Second generation framing structure, channel coding and modulation systems for Broadcasting, Interactive Services, News Gathering and other broadband satellite applications; Part 1: DVB-S2*. 2014.

[22] 3GPP. *3GPP TS 38.211. 5G; NR; Physical channels and modulation (3GPP TS 38.211 version 15.2.0 Release 15)*. July 2018.

[23] *Recommendation ITU-R SM.1541-6. Unwanted emissions in the out-of-band domain*. Aug. 2015.

[24] *ETSI TS 138 101-1. 5G; NR; User Equipment (UE) radio transmission and reception; Part 1: Range 1 Standalone (3GPP TS 38.101-1 version 15.3.0 Release 15)*. Oct. 2018.

[25] 3GPP. *5G;NR;Multiplexing and channel coding(3GPP TS 38.212 version 15.6.0 Release 15)*.

[26] IEEE. *IEEE P802.11 Wireless LANs. TGad Evaluation Methodology*. Jan. 20, 2009.

[27] S. Daumont, B. Rihawi and Y. Lout. Root-Raised Cosine filter influences on PAPR distribution of single carrier signals. *2008 3rd International Symposium on Communications, Control and Signal Processing*. 2008 3rd International Symposium on Communications, Control and Signal Processing. Mar. 2008, 841–845. DOI: 10.1109/ISCCSP.2008.4537340.

[28] 3GPP TSG RAN WG4 Meeting #82. *Potential Response to LS on pi/2 BPSK with frequency domain pulse shaping.* Feb. 2017.

[29] L. Bahl, J. Cocke, F. Jelinek and J. Raviv. Optimal decoding of linear codes for minimizing symbol error rate (Corresp.) *IEEE Transactions on Information Theory* 20.2 (Mar. 1974), 284–287. ISSN: 1557-9654. DOI: 10.1109/TIT.1974.1055186.

[30] 3GPP. *5G;NR;Physical layer procedures for data(3GPP TS 38.214 version 15.7.0 Release 15)*. Oct. 2019.

[31] 3GPP. *LTE;5G;Study on channel model for frequency spectrum above 6 GHz(3GPP TR 38.900 version 14.2.0 Release 14)*.

A EXAMPLES OF CPSK MAPPING TABLES

In this appendix, examples bit to symbol mapping tables for CPSK are shown (Tables A.1 to A.6). Note that the bit to symbol mapping can be freely defined, these tables are just presented to exemplify the mapping.

Table A.1. Bit to symbol mapping example for C5PSK with 3 options.

Input bits	Previous symbol									
	s_0		s_1		s_2		s_3		s_4	
000	s_0	s_1	s_1	s_2	s_2	s_3	s_3	s_4	s_4	s_0
001	s_0	s_4	s_1	s_0	s_2	s_1	s_3	s_2	s_4	s_3
010	s_1	s_2	s_2	s_3	s_3	s_4	s_4	s_0	s_0	s_1
011	s_4	s_3	s_0	s_4	s_1	s_0	s_2	s_1	s_3	s_2
100	s_1	s_0	s_2	s_1	s_3	s_2	s_4	s_3	s_0	s_4
101	s_4	s_0	s_0	s_1	s_1	s_2	s_2	s_3	s_3	s_4
110	s_1	s_1	s_2	s_2	s_3	s_3	s_4	s_4	s_0	s_0
111	s_4	s_4	s_0	s_0	s_1	s_1	s_2	s_2	s_3	s_3

Table A.2. Bit to symbol mapping example for C6PSK with 3 options.

Input bits	Previous symbol											
	s_0		s_1		s_2		s_3		s_4		s_5	
000	s_0	s_1	s_1	s_2	s_2	s_3	s_3	s_4	s_4	s_5	s_5	s_0
001	s_0	s_5	s_1	s_0	s_2	s_1	s_3	s_2	s_4	s_3	s_5	s_4
010	s_1	s_2	s_2	s_3	s_3	s_4	s_4	s_5	s_5	s_0	s_0	s_1
011	s_5	s_4	s_0	s_5	s_1	s_0	s_2	s_1	s_3	s_2	s_4	s_3
100	s_1	s_0	s_2	s_1	s_3	s_2	s_4	s_3	s_5	s_4	s_0	s_5
101	s_5	s_0	s_0	s_1	s_1	s_2	s_2	s_3	s_3	s_4	s_4	s_5
110	s_1	s_1	s_2	s_2	s_3	s_3	s_4	s_4	s_5	s_5	s_0	s_0
111	s_5	s_5	s_0	s_0	s_1	s_1	s_2	s_2	s_3	s_3	s_4	s_4

Table A.3. *Bit to symbol mapping example for C7PSK with 3 options.*

Input bits	Previous symbol												
	s_0		s_1		s_2		s_3		s_4		s_5		s_6	
000	s_0	s_1	s_1	s_2	s_2	s_3	s_3	s_4	s_4	s_5	s_5	s_6	s_6	s_0
001	s_0	s_6	s_1	s_0	s_2	s_1	s_3	s_2	s_4	s_3	s_5	s_4	s_6	s_5
010	s_1	s_2	s_2	s_3	s_3	s_4	s_4	s_5	s_5	s_6	s_6	s_0	s_0	s_1
011	s_6	s_5	s_0	s_6	s_1	s_0	s_2	s_1	s_3	s_2	s_4	s_3	s_5	s_4
100	s_1	s_0	s_2	s_1	s_3	s_2	s_4	s_3	s_5	s_4	s_6	s_5	s_0	s_6
101	s_6	s_0	s_0	s_1	s_1	s_2	s_2	s_3	s_3	s_4	s_4	s_5	s_5	s_6
110	s_1	s_1	s_2	s_2	s_3	s_3	s_4	s_4	s_5	s_5	s_6	s_6	s_0	s_0
111	s_6	s_6	s_0	s_0	s_1	s_1	s_2	s_2	s_3	s_3	s_4	s_4	s_5	s_5

Table A.4. *Bit to symbol mapping example for C8PSK with 3 options.*

Input bits	Previous symbol															
	s_0		s_1		s_2		s_3		s_4		s_5		s_6		s_7	
000	s_0	s_1	s_1	s_2	s_2	s_3	s_3	s_4	s_4	s_5	s_5	s_6	s_6	s_7	s_7	s_0
001	s_0	s_7	s_1	s_0	s_2	s_1	s_3	s_2	s_4	s_3	s_5	s_4	s_6	s_5	s_7	s_6
010	s_1	s_2	s_2	s_3	s_3	s_4	s_4	s_5	s_5	s_6	s_6	s_7	s_7	s_0	s_0	s_1
011	s_7	s_6	s_0	s_7	s_1	s_0	s_2	s_1	s_3	s_2	s_4	s_3	s_5	s_4	s_6	s_5
100	s_1	s_0	s_2	s_1	s_3	s_2	s_4	s_3	s_5	s_4	s_6	s_5	s_7	s_6	s_0	s_7
101	s_7	s_0	s_0	s_1	s_1	s_2	s_2	s_3	s_3	s_4	s_4	s_5	s_5	s_6	s_6	s_7
110	s_1	s_1	s_2	s_2	s_3	s_3	s_4	s_4	s_5	s_5	s_6	s_6	s_7	s_7	s_0	s_0
111	s_7	s_7	s_0	s_0	s_1	s_1	s_2	s_2	s_3	s_3	s_4	s_4	s_5	s_5	s_6	s_6

Table A.5. *Bit to symbol mapping example for C5PSK with 4 options. Even/odd symbol index*

Input bits	Previous symbol				
	s_0	s_1	s_2	s_3	s_4
00	s_0	s_1	s_2	s_3	s_4
01	s_1	s_2	s_3	s_4	s_0
10	s_4	s_0	s_1	s_2	s_3
11	s_2/s_3	s_3/s_4	s_4/s_0	s_0/s_1	s_1/s_2

Table A.6. *Bit to symbol mapping example for C6PSK with 4 options. Even/odd symbol index*

Input bits	Previous symbol					
	s_0	s_1	s_2	s_3	s_4	s_5
00	s_0	s_1	s_2	s_3	s_4	s_5
01	s_1	s_2	s_3	s_4	s_5	s_0
10	s_5	s_0	s_1	s_2	s_3	s_4
11	s_2/s_4	s_3/s_5	s_4/s_0	s_5/s_1	s_0/s_2	s_1/s_3

B MAXIMUM PA OUTPUT POWER

Detailed tables of the maximum PA output power per modulation are shown in this appendix.

Table B.1. *Maximum output power per modulation fulfilling all requirements for the UL*

Modulation	ACLR [dB]	EVM [%]	Pout [dBm]	IBO [dB]	Limiting factor
QPSK	23.4	9	21.09	-8.1	Mask
[1-D]π/2-4PAM	23.8	15.4	23.56		Mask
C5PSK/4	23.4	9.2	22.79	-11.9	99 % of power inside channel BW
C6PSK/4	23.5	9.3	24.17	-16.9	Mask
C7PSK/4	24.1	10.1	25	-25	Mask
C8PSK/4	25.6	8.7	25.26	-45	Saturation level of PA
$\pi/4$**-QPSK**$_{\alpha=0.25}$	23.6	7.50	22.15	-10.5	99 % of power inside channel BW
C5PSK/4$_{\alpha=0.25}$	25	10.1	24.07	-16.5	99 % of power inside channel BW
C6PSK/4$_{\alpha=0.25}$	26	9.8	25.26	-45	Saturation level of PA
C7PSK/4$_{\alpha=0.25}$	29	9.2	25.26	-45	Saturation level of PA
C8PSK/4$_{\alpha=0.25}$	31.4	6.3	25.26	-45	Saturation level of PA
C4PSK/3	23.3	9.3	23.28	-13.3	99 % of power inside channel BW
C5PSK/3	23.9	9	24.73	-20.9	Mask
C6PSK/3	25.3	7.8	25.26	-45	Saturation level of PA
C7PSK/3	27.3	6.7	25.26	-45	Saturation level of PA
C8PSK/3	29.5	6.2	25.26	-45	Saturation level of PA
[1-D]π/2-BPSK	28.3	16.3	25.26	-45	Saturation level of PA

Table B.2. *Maximum output power per modulation fulfilling all requirements for the DL*

Modulation	ACLR [dB]	EVM [%]	Pout [dBm]	IBO [dB]	Limiting factor
QPSK	28	5.6	18	-3.2	ACLR $\geq$ 28 dB
[1-D]π/2-4PAM	28	7	21.14	-8.7	ACLR $\geq$ 28 dB
C5PSK/4	28	5.8	19.72	-5.6	ACLR $\geq$ 28 dB
C6PSK/4	28	5.7	21.27	-8.2	ACLR $\geq$ 28 dB
C7PSK/4	28	6.4	22.65	-11.2	ACLR $\geq$ 28 dB
C8PSK/4	28	6.4	23.75	-14.7	ACLR $\geq$ 28 dB
$\pi/4$-QPSK$_{\alpha=0.25}$	28	6.00	20.2	-6.5	ACLR $\geq$ 28 dB
C5PSK/4$_{\alpha=0.25}$	28	7.2	22.35	-10.6	ACLR $\geq$ 28 dB
C6PSK/4$_{\alpha=0.25}$	28	7.8	24.21	-17	ACLR $\geq$ 28 dB
C7PSK/4$_{\alpha=0.25}$	29	9.2	25.26	-45	Saturation level of PA
C8PSK/4$_{\alpha=0.25}$	31.4	6.3	25.26	-45	Saturation level of PA
C4PSK/3	28	5.6	20.17	-6.3	ACLR $\geq$ 28 dB
C5PSK/3	28	5.6	22.11	-9.4	ACLR $\geq$ 28 dB
C6PSK/3	28	5.8	23.73	-14.6	ACLR $\geq$ 28 dB
C7PSK/3	28	6.4	25.09	-27	ACLR $\geq$ 28 dB
C8PSK/3	29.5	6.2	25.26	-45	Saturation level of PA
[1-D]π/2-BPSK	28.3	16.3	25.26	-45	Saturation level of PA